The Thesis committee for Mason Daily Phillips
Certifies that this is the approved version of the following thesis:

Geophysical data registration using modified plane-wave destruction filters

APPROVED BY

SUPERVISING COMMITTEE:

Sergey Fomel, Supervisor

Mrinal Sen

Clark Wilson

Geophysical data registration using modified plane-wave destruction filters

by

Mason Daily Phillips, B.S.Geo.Sci.

THESIS

Presented to the Faculty of the Graduate School of

The University of Texas at Austin

in Partial Fulfillment

of the Requirements

for the Degree of

Master of Science in Geological Sciences

THE UNIVERSITY OF TEXAS AT AUSTIN

May 2017

Dedicated to my friends, family, and mentors who have provided support and encouragement

Acknowledgments

I am deeply grateful for the many individuals who have supported me over the years and contributed to the production of this thesis.

First and foremost, I would like to thank my advisor, Sergey Fomel. I have been fortunate to have him as an advisor and have learned a great deal from his guidance and patience. He gave me the freedom to operate independently and learn through example and experience, but was always available to provide guidance when necessary. His wealth of knowledge and acumen for scientific research, inquiry, and discovery are inspiring. We collaborated on Phillips et al. (2016), Phillips and Fomel (2016), and Phillips and Fomel (2017b), parts of which are used in this thesis, as well as Phillips and Fomel (2017a). I appreciate everything he has taught me.

I would like to thank committee members, Mrinal Sen and Clark Wilson for their insightful feedback to this thesis. Mrinal's expertise in seismic theory, inversion, and imaging, as demonstrated though his lectures, was critical to my research. Similarly, thanks to Clark for introducing me to signal processing and numerical analysis and for giving me the opportunity to help him teach three courses. I would also like to thank the many other professors and mentors who have invested numerous hours teaching, guiding, and encouraging me over the years, particularly Kyle Spikes, Peter Hennings, Steve Grand, Heather DeShon, Luc Lavier, John Benson, and Adrian Muñoz. Additional thanks to Tom Hess and Karl Schleicher for their advice and expertise in seismic data processing. My thanks also go to academic advisors, Philip Guerrero and Jessica Hust, for making my experience at the University of Texas at

Austin more enjoyable.

Sergey has created a world-class environment for addressing challenging problems and developing of new ideas in geophysics. Thanks to my friends and colleagues at the Texas Consortium of Computational Seismology (TCCS), Sean Bader, Yangkang Chen, Luke Decker, Sarah Greer, Parvaneh Karimi, Yenming Lai, Dmitrii Merzlikin, Kelly Regimbal, Yunzhi Shi, Yanadet Sripanich, Junzhe Sun, Ryan Swindeman, Xinming Wu, Zhiguang Xue, Yunan Yang, Hejun Zhu, and Tieyuan Zhu. Each of you have been enlightening and inspirational during my time working with you. I have been fortunate to be surrounded by technical experts who have been tremendously supportive, helpful, and encouraging. Special thanks to my local collaborators, Ryan, Dmitrii, and Xinming. We collaborated on Phillips et al. (2016) and Merzlikin et al. (2017).

The computational examples reported in this thesis are reproducible using the Madagascar software package, an open-source environment designed for multidimensional data analysis (Fomel et al., 2013). I am grateful to all of the Madagascar developers who provided the tools necessary to complete the work in this thesis.

Thanks to Paul Hatchell and Sudhish Bakku of Shell Projects & Technology Areal Monitoring Team for inspiring discussions about time-lapse seismic data analysis. Thanks to the National Energy Technology Laboratory (NETL), the Southeast Regional Carbon Sequestration Partnership (SECARB), and Denbury Resources for providing the time-lapse seismic data example from the Cranfield CO_2 injection experiment. Thanks to Mobil Oil, the Nova Scotia Department of Energy, the Canada Offshore Petroleum Board, and the New Zealand Petroleum and Minerals for providing the other field data used in this paper to the SEG open data reposi-

tory (`http://wiki.seg.org/wiki/Open_data`). Thanks to the sponsors of the Texas Consortium for Computational Seismology (TCCS) and the Department of Geological Sciences for financial support.

Most importantly, none of this would have been possible without my parents, Stan and Margie, and sister, Megan. They receive my deepest gratitude for their constant encouragement, and support throughout the years.

Geophysical data registration using modified plane-wave destruction filters

Mason Daily Phillips, M.S.Geo.Sci.

The University of Texas at Austin, 2017

Supervisor: Sergey Fomel

I propose a method to efficiently measure local shifts, slopes, and scaling functions between seismic traces using modified plane-wave destruction filters. Plane-wave destruction can efficiently measure shifts of less than a few samples, making this algorithm particularly effective for detecting small shifts. When shifts are large, amplitude-adjusted plane-wave destruction can also be used to refine shift estimates obtained by other methods.

Amplitude-adjusted plane-wave destruction separates estimation of local shifts and amplitude weights, allowing the time-shift to be measured more accurately. This algorithm has clear applications to geophysical data registration problems, including time-lapse image registration, multicomponent image registration, automatic gather flattening, automatic seismic-well ties, and image merging. The effectiveness of this algorithm in predicting shifts associated with fluid migration, wave mode conversions, and anisotropy and amplitude gradients associated with amplitude variations

with offset or angle is demonstrated by applying the algorithm to a synthetic trace, a time-lapse field data example from the Cranfield CO_2 sequestration project, a multi-component field data example from West Texas, and the Mobil AVO prestack seismic data.

Finding correspondence between different parts of the same dataset falls into the same category of problems as local shift estimation. Computation of structure-oriented amplitude gradients for attribute-assisted interpretation requires the estimation of local slopes by correlating reflections between neighboring seismic traces in an image. One of the major challenges of interpreting seismic images is the delineation of reflection discontinuities that are related to geologic features, such as faults, channels, salt boundaries, and unconformities. Visually prominent reflection features often overshadow these subtle discontinuous features which are critical to understanding the structural and depositional environment of the subsurface. For this reason, precise manual interpretation of these reflection discontinuities in seismic images can be tedious and time-consuming, especially when data quality is poor. Discontinuity enhancement attributes are commonly used to facilitate the interpretation process by enhancing edges in seismic images and providing a quantitative measure of the significance of discontinuous features. These attributes require careful pre-processing to maintain geologic features and suppress acquisition and processing artifacts which may be artificially detected as a geologic edge.

The plane-wave Sobel filter cascades plane-wave destruction filters with plane-wave shaping in the transverse direction to compute an enhanced discontinuity attribute. The plane-wave Sobel attribute can be applied directly to a seismic image to efficiently and effectively enhance discontinuous features, or to a coherence image to create a sharper and more detailed image. I demonstrate the effectiveness of this

method by applying it to two field data sets from offshore New Zealand and offshore Nova Scotia with several faults and channel features and compare the results to other coherence attributes.

Table of Contents

List of Figures

Chapter 1

Introduction

Data registration refers to transformation of multiple different data sets or parts of the same data set recorded by different instruments, at different times, or at different locations into a common coordinate system by finding correspondences between data points and aligning them. Registration is required when comparing or integrating multiple data sets. The term "registration" was originally coined in medical imaging (Maintz and Viergever, 1998), but has applications in situations where multiple data sets must be analyzed, including computer vision (Horn and Schunck, 1981), target recognition (Bar-Shalom, 1990), satellite image analysis (Kim and Im, 2003; Nuth and Kääb, 2011), and geophysical data processing (Fomel et al., 2005; Fomel and Jin, 2009; Baek et al., 2014; Zhang et al., 2014).

Many data analysis problems in geophysics involve measuring relative shifts between two or more data sets, including time-lapse image registration and multi-component image registration. Shifts between different parts of the same data set correspond to local slopes and fall into the same category of problems. Estimation of local slopes has clear applications in automatic gather flattening and fault detection in seismic images. Though there are more applications (Fomel, 2002), in this thesis, I will focus on these four topics. Greer and Fomel (2017) overviews recent advances in image merging.

Over the past 25 years, time-lapse seismic monitoring has evolved into the standard method to detect spatial fluid changes in the subsurface (Lumley, 2001). In some locations, permanent stations have been installed for continuous time-lapse monitoring (Berron et al., 2015). In time-lapse seismic monitoring, sensitive acquisition and processing is required to detect small shifts induced by fluid migration.

Multicomponent receivers, as well as SH sources, allow S-waves to be processed along with P-waves to create multiple images of the subsurface. Like time-lapse seismic images, multicomponent seismic images must be registered to the same frame of reference for proper interpretation (Hardage et al., 2011). In multicomponent image registration, it is important to measure shifts to high resolution to ensure that the images are in the same reference frame. Furthermore, useful attributes can be computed from multicomponent timeshifts for fracture characterization (Tsvankin, 1997).

Prestack seismic data is routinely flattened using anisotropic moveout corrections; however, it is still difficult to eliminate all reflection curvature while maintaining a physically reasonable models of subsurface anisotropy and velocity. Flat gathers also dramatically simplify the extraction of prestack attributes, such as amplitude intercepts and gradients, for AVO analysis (Shuey, 1985; Castagna et al., 1998). Dynamic gather flattening algorithms are generally not constrained by physics and are most suitable for refining gathers that are already nearly flat. Also, commonly used algorithms typically use local cross-correlation or dynamic time warping to flatten gathers. Conventional algorithms do not explicitly address amplitude variations as a function of offset or angle in the estimation of residual moveout corrections.

Discontinuity enhancement attributes are among the most widely used seismic

attributes today (Chopra and Marfurt, 2007). These attributes are generally post-stack image domain calculations of the similarity or dissimilarity along a horizon or time-slice between a neighborhood of adjacent seismic traces. Discontinuous features, such as faults, channels, salt boundaries, unconformities, mass-transport complexes, and subtle stratigraphic features can be identified as area of low similarity. Such attributes are powerful interpretation tools that make detailed interpretation of previously indistinguishable features possible. Orientation of amplitude gradient attributes along seismic structures for discontinuity enhancement requires the estimation of local slopes of seismic images.

In this thesis, I adopt and extend plane-wave destruction (Fomel, 2002) for automatic estimation of time-variant shifts and scaling functions between seismic traces. The proposed amplitude-adjusted plane-wave destruction filters effectively estimate regularized time-shifts associated with fluid migration, mode conversions, and anisotropy in the presence of noise and amplitude variations. I test the proposed algorithm using synthetic and field data.

I subsequently propose to modify the classic Sobel filter (Sobel and Feldman, 1968) to explicitly follow seismic structures (Phillips and Fomel, 2017b). I modify the Sobel filter by replacing the discrete differential operator with linear plane-wave destruction (Fomel, 2002) and triangular smoothing with plane-wave shaping (Fomel, 2007b; Swindeman and Fomel, 2015). This method is particularly efficient because it does not require computation of the eigenvectors of the covariance matrix or structure-tensor. Local slopes are instead estimated using accelerated plane-wave destruction (Chen et al., 2013a). I further modify the Sobel filter by orienting the filter along the azimuth perpendicular to discontinuities by following the fast azimuth scanning workflow proposed by Merzlikin et al. (2016). I test this modification on benchmark

3D seismic images from offshore New Zealand and Nova Scotia, Canada and compare the results with those from previously proposed coherence attributes.

THESIS OUTLINE

In chapter 2, I review conventional geophysical data registration techniques, including local cross-correlation, dynamic time-warping, local similarity, and gradient structure tensors and discuss the scenarios where each of these algorithms succeed and fail. I subsequently review plane-wave destruction (Fomel, 2002) and introduce the first modification of the algorithm, amplitude-adjusted plane-wave destruction.

In chapter 3, I apply amplitude-adjusted plane-wave destruction filters to a synthetic example, a time-lapse example from the Cranfield CO_2 injection experiment, and a multicomponent example from a West Texas carbonate field.

In chapter 4, I apply amplitude adjusted plane-wave destruction filters to flatten prestack seismic data to correct for non-hyperbolic moveout associated with anisotropy in the presence of AVO anomalies, noise, and an imperfect initial subsurface velocity structure. I evaluate the effectiveness of this algorithm using a complex synthetic midpoint gather and the famous Mobil AVO seismic data.

In chapter 5, I introduce the second modification of plane-wave destruction filters, the plane-wave Sobel filter. This filter provides an image with isolated discontinuous features commonly interpreted from seismic images, including channels and faults. The effectiveness of this attribute is evaluated using two 3D marine seismic volumes from offshore Nova Scotia and New Zealand. The results are compared to other commonly used attributes and their performance is evaluated.

In chapter 6, I summarize the work presented in this thesis with a brief discussion of the results and future applications.

Chapter 2

Review of seismic attribute and plane-wave destruction

CROSSCORRELATION

Crosscorrelation is a measure of similarity between two digital signals systematically calculated at regularly spaced lags. This attribute has been used in countless geophysical applications which involve pattern recognition. It is defined below as the sum of the product of two digital signals where one signal has been statically shifted

$$\gamma(\tau) = \sum_{t=0}^{N_t} f(t)g(t+\tau) \ , \tag{2.1}$$

where f and g are zero mean digital signals of length N_t and τ is a time shift.

Normalized crosscorrelation can be computed over small windows to approximate the local correlation attribute. An arbitrary weighting function W_t (Gaussian, box, triangle, etc.) can be applied to each sum.

$$\gamma(\tau) = \frac{\sum\limits_{t=\tau-\Delta\tau}^{\tau+\Delta\tau} W_t f(t)g(t+\tau)}{\sqrt{\sum\limits_{t=\tau-\Delta\tau}^{\tau+\Delta\tau} W_t f^2(t)}\sqrt{\sum\limits_{t=\tau-\Delta\tau}^{\tau+\Delta\tau} W_t g^2(t)}} \ , \tag{2.2}$$

where $\Delta\tau$ is the lag window over which the normalized crosscorrelation attribute is computed.

By selecting the lag which corresponds to the highest correlation coefficient γ at each sample, the warping path which maximizes the local crosscorrelation can be

estimated; however, this warping path consists of only integer time-shifts. To alleviate this "stair-stepping" artifact, a parabola can be constructed using least squares to fit the lag which corresponds to the peak correlation coefficient and its two immediate neighbors. The extreme point is calculated analytically and chosen to be the floating-point precision time-shift (Figure 2.1).

Hale (2006) proposed an analagous algorithm which successfully predicts timeshifts associated with reservoir compaction. Crosscorrelation based algorithms are surprisingly robust given their simplicity, making them an attractive choice for geophysical data registration problems (Rickett and Lumley, 2001). However, Kanu et al. (2016) show that there are more reliable timeshift estimation algorithms in the application of time-lapse reservoir monitoring.

DYNAMIC TIME WARPING

Dynamic time warping is an algorithm for measuring similarity between two time series (Sakoe and Chiba, 1978). It is particularly effective for comparing time-series which are similar, but temporally stretched or squeezed. This algorithm was originally developed for speech recognition, but has found numerous applications in image processing.

Dynamic time warping determines a warping path which optimally aligns two signals. This path is determined by minimizing the alignment error e

$$e(t) = \arg\min_{\tau} \left(f(t) - g(t+\tau)\right)^2 \ . \tag{2.3}$$

Traditional dynamic time warping may provide a solution which requires physically unreasonable time-shifts, so the minimization of alignment errors must be con-

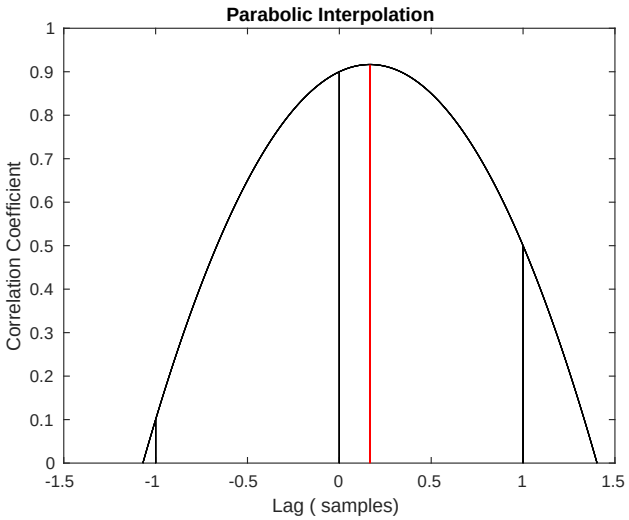

Figure 2.1: An illustration of parabolic interpolation. Maximum correlation is achieved at zero lag. A parabola is constructed which connects the max correlation value to its two immediate neighbors. The extreme point of the parabola (red) approximates the true time-shift required to maximize the similarity of the waveforms. ch02-review/. parabola

strained. Similar to the slope constraint of Sakoe and Chiba (1978), Hale (2013a) proposes to impose a strain limit on the solution. This effectively windows the boundary over which alignment errors are calculated. Additionally, Hale (2013a) smooths the map of alignment errors before selecting the optimal warping path to alleviate high frequency oscillations in the solution.

Dynamic time warping has been successfully applied to many geophysical data registration problems. Hale (2013a) uses the algorithm for multicomponent image registration and estimation of fault throws from seismic images. Qian et al. (2016) modifies the algorithm to use an adaptive window for automatic gather flattening. Munoz and Hale (2012) and Herrera and van der Baan (2012) use dynamic time warping for automatic seismic-well ties. Wu and Caumon (2016) extends the work of Munoz and Hale (2012) for automatic simultaneous multiple seismic-well ties.

Dynamic time warping can achieve a good match between two time series, but commonly produces physically unreasonable timeshifts. Further, dynamic time-warping cannot reliably measure small time-shifts (less than 1 sample). In applications such as time-lapse image registration, time-shifts are commonly very small (less than one sample). Dynamic time warping may not provide sufficient resolution to effectively address this problem.

LOCAL SIMILARITY

As the name suggests, local similarity (Fomel, 2007a) is a local attribute for measuring the similarity between two digital signals. It can be represented as the

product of two local attributes $\gamma^2(t) = p(t)q(t)$ where

$$p(\tau) = \frac{\sum_{t=0}^{N_t} f(t)g(t+\tau)}{\sum_{t=0}^{N_t} g^2(t)} \tag{2.4}$$

and

$$q(\tau) = \frac{\sum_{t=0}^{N_t} f(t)g(t+\tau)}{\sum_{t=0}^{N_t} f^2(t)} \ , \tag{2.5}$$

are the solutions to the least-squares minimization problems

$$\min_p \sum_{t=0}^{N_t} \left(f(t) - p(t)g(t)\right)^2 \tag{2.6}$$

and

$$\min_q \sum_{t=0}^{N_t} \left(g(t) - q(t)f(t)\right)^2 \ . \tag{2.7}$$

Instead of using local windows, the problem can regularized by shaping regularization (Fomel, 2007b). Local similarity has found successful applications to multicomponent image registration (Fomel et al., 2005), time-lapse image registration (Fomel and Jin, 2009; Zhang et al., 2013, 2014), automatic seismic-well ties (Herrera et al., 2014), and image merging (Greer and Fomel, 2017).

GRADIENT STRUCTURE TENSOR

On of the most common algorithms for seismic reflection slope estimation is based on the eigendecomposition of the gradient structure tensor of a seismic image. In 3D, the structure tensor $\mathbf{S}$ is a 3×3 matrix constructed as the smooth outer product of image gradients in each dimension.

$$\mathbf{S} = \left\langle \nabla\nabla^T \right\rangle = \begin{pmatrix} \langle \partial_{xx} \rangle & \langle \partial_{xy} \rangle & \langle \partial_{xz} \rangle \\ \langle \partial_{yx} \rangle & \langle \partial_{yy} \rangle & \langle \partial_{yz} \rangle \\ \langle \partial_{zx} \rangle & \langle \partial_{zy} \rangle & \langle \partial_{zz} \rangle \end{pmatrix} , \tag{2.8}$$

where $\langle \cdot \rangle$ represents Gaussian smoothing. This matrix can be represented by the sum of the outer product of its eigenvectors weighted by their corresponding eigenvalues computed using singular value decomposition.

$$\mathbf{S} = \sum_{i=1}^{3} \lambda_i \mathbf{u}_i \mathbf{u}_i^T , \tag{2.9}$$

where λ_i and $\mathbf{u}_i$ are the i^{th} eigenvalue and eigenvector pair. The order of the eigenvectors is defined such that $\lambda_1 \geq \lambda_2 \geq \lambda_3$. $\mathbf{u}_1$ corresponds to the orientation which maximizes the directional image gradient; $\mathbf{u}_3$ corresponds to the orientation which minimizes the directional image gradient in the plane whose norm is defined as $\mathbf{u}_1$. When applied to a seismic image with laterally continuous features, $\mathbf{u}_1$ is oriented normal to seismic reflection events and $\mathbf{u}_2$ and $\mathbf{u}_3$ define the local plane which closest approximates the seismic reflection structure. This assumption fails when discontinuous geological features, such as channels, faults, unconformities, and salt boundaries are expressed in seismic images. Hale (2009b) and Wu (2017) orient anisotropic smoothing filters along seismic structures using this formulation to compute discontinuity enhancing attributes.

PLANE-WAVE DESTRUCTION

Finite-difference plane-wave destruction filters (Fomel, 2002) perform well in applications such as noise separation, interpolation, and fault detection. The local-plane wave model assumes seismic traces can be effectively predicted by dynamically shifting adjacent seismic traces. This model is useful for seismic data characterization

and is the basis for plane-wave destruction filters. The local plane-wave differential equation is defined by Claerbout (1992) as

$$\frac{\partial u}{\partial x} + p\frac{\partial u}{\partial t} = 0 \ , \tag{2.10}$$

where u is the seismic wavefield and p is the temporally and spatially variable local slope. The optimal local slopes are determined by minimizing the regularized plane-wave residual (Fomel, 2002).

High order plane-wave destruction filters are described in the Z-transform notation as

$$C(p, Z_1, Z_2) = B(p, Z_1^{-1}) - Z_2 B(p, Z_1) \ , \tag{2.11}$$

where C is the plane-wave destruction filter, B is an all-pass filter, p is the local slope, and Z_i is a local shift in the i^{th} dimension.

The coefficients of third and fifth order expansions of B are defined by Fomel (2002) as

$$B_3(p) = \begin{pmatrix} \dfrac{(1-p)(2-p)}{12} \\ \dfrac{(2+p)(2-p)}{6} \\ \dfrac{(1+p)(2+p)}{12} \end{pmatrix} \tag{2.12}$$

and

$$B_5(p) = \begin{pmatrix} \frac{(1-p)(2-p)(3-p)(4-p)}{1680} \\ \frac{(4-p)(2-p)(3-p)(4+p)}{420} \\ \frac{(4-p)(3-p)(3+p)(4+p)}{280} \\ \frac{(4-p)(2+p)(3+p)(4+p)}{420} \\ \frac{(1+p)(2+p)(3+p)(4+p)}{1680} \end{pmatrix}, \tag{2.13}$$

respectively and correspond to Thiran filters (Thiran, 1971; Chen et al., 2013b)

Plane-wave destruction filters perform well in the application of slope estimation, fault detection, trace interpolation, and noise separation in seismic images; however, these filters require laterally consistent amplitudes. It is important to allow subtle amplitude variations in the application of these types of filters to images with lateral amplitude variations.

AMPLITUDE-ADJUSTED PLANE-WAVE DESTRUCTION FILTERS

In the slope estimation application of plane-wave destruction filters, the proper slope may be difficult to estimate in the presense of lateral amplitude variations. Though the assumption of consistent lateral amplitudes may not be a limiting factor in local slope estimation in seismic images, in the velocity independent imaging workflow, seismic reflections are flattened in the offset, angle, or image domain using the local slope of seismic reflection events in gathers (Fomel, 2007c). Amplitude variations commonly exist as a function of offset, angle or azimuth in gathers and are crucial

for interpretation of seismic data; therefore, it is important to consider these variations when flattening gathers (Phillips, 2017). Similarly, amplitude variations exist between time-lapse due to changes in fluid saturation. Ignoring amplitudes when estimating 4D timeshifts may produce arbitrarily large spurious timeshift estimates at the reservoir, particularly when the layers are below seismic resolution (MacBeth et al., 2016).

I propose to estimate local scaling functions and spatially variable temporal shifts by modifying plane-wave destruction (Fomel, 2002) to include scaling. A scaling function is incorporated in the description of high-order plane-wave destruction filters. I modify this formulation to incorporate a scaling function as follows (Phillips and Fomel, 2016):

$$D(a, p, Z_1, Z_4) = B(p, Z_1^{-1}) - aZ_2B(p, Z_1) \ , \tag{2.14}$$

where a is a scaling coefficient. In the matrix-vector notation, equation (2.14) can be expressed as

$$\mathbf{D}(\mathbf{a}, \mathbf{p})\mathbf{d} = \mathbf{B}_l(\mathbf{p})\mathbf{d} - \text{diag}(\mathbf{a})\mathbf{B}_r(\mathbf{p})\mathbf{d} \ , \tag{2.15}$$

where $\mathbf{B}$ and $\mathbf{D}$ denote the convolution operator with the filters B and D, respectively, and $\mathbf{d}$ is the concatenation of multiple datasets ($\mathbf{d} = \sum_{i=0}^{N-1} d_i Z_4^i$). r and l denote the right and left hand side of the polynomial filter B. Our goal for the warped and scaled data is to match the base data, therefore we seek to minimize the output

$$\mathbf{D}(\mathbf{a}, \mathbf{p})\mathbf{d} \approx 0. \tag{2.16}$$

The dependence of $\mathbf{D}$ on $\mathbf{a}$ is linear, however $\mathbf{p}$ enters in a nonlinear way (Chen et al., 2013a). It is convenient to separate the problem into a linear and nonlinear part and use the variable projection technique (Golub and Pereyra, 1973; Kaufman, 1975).

The proposed algorithm is outlined below.

1. Set $\mathbf{p}_0 = \mathbf{0}$ and $\mathbf{a}_0 = \mathbf{1}$
2. Hold the scale $\mathbf{a}_n$ constant and compute the shift $\mathbf{p}_n$ using accelerated plane-wave destruction (Chen et al., 2013a)
3. Shift the traces image using $\mathbf{p}_n$
4. Hold the shift $\mathbf{p}_n$ constant and compute the amplitude ratio $\mathbf{a}_n$ by the smooth division of the left and right side of the plane-wave destruction filter $\mathbf{D}$ in equation (2.15):
$$\mathbf{a}_n = \left\langle \frac{\mathbf{B}_l(\mathbf{p}_n)\mathbf{d}}{\mathbf{B}_r(\mathbf{p}_n)\mathbf{d}} \right\rangle \tag{2.17}$$
5. Scale the gather using $\mathbf{a}_n$
6. Iterate until convergence (return to step 2)

This algorithm efficiently shifts and scales seismic traces to match associated traces. The estimated shifts and scaling weights are constrained to be smooth using shaping regularization (Fomel, 2007b).

SOBEL FILTER

The traditional Sobel operator approximates a smoothed gradient of the image intensity function. It is defined as the convolution of an image with two 3×3 filters. The first of these filters (S_i) differentiates in the inline direction and averages in the crossline direction. The second filter (S_x) differentiates in the crossline direction and averages in the inline direction.

$$S_i = \begin{bmatrix} -1 & 0 & 1 \\ -2 & 0 & 2 \\ -1 & 0 & 1 \end{bmatrix} = \begin{bmatrix} 1 \\ 2 \\ 1 \end{bmatrix} \begin{bmatrix} -1 & 0 & 1 \end{bmatrix} \tag{2.18}$$

$$S_x = S_i^T = \begin{bmatrix} -1 & -2 & -1 \\ 0 & 0 & 0 \\ 1 & 2 & 1 \end{bmatrix} \tag{2.19}$$

In the Z-transform notation, filters (1) and (2) can be expressed as

$$\begin{array}{l} S_i(Z_i, Z_x) = (Z_x + 2 + Z_x^{-1})(Z_i - Z_i^{-1}) \\ S_x(Z_i, Z_x) = (Z_x - Z_x^{-1})(Z_i + 2 + Z_i^{-1}) \end{array} , \tag{2.20}$$

where Z_j is a phase shift in the j direction.

The inline and crossline images are combined to approximate the magnitude of the image gradient (Chopra and Marfurt, 2007) where $\mathbf{d}$ is the data and $\mathbf{S}_i$ and $\mathbf{S}_x$ are convolution operators with the filters S_i and S_x, respectively.

$$\|\nabla \mathbf{d}\| \approx \sqrt{(\mathbf{S}_i \mathbf{d})^2 + (\mathbf{S}_x \mathbf{d})^2} \tag{2.21}$$

This filter can be applied to images to enhance discontinuous features; however, when applied to seismic images, it is important to orient the filter along seismic reflection structures to avoid enhancement of dipping reflection events (Phillips and Fomel, 2017b).

Chapter 3

Seismic image registration using amplitude-adjusted plane-wave destruction

I propose a method to efficiently measure timeshifts and scaling functions between seismic images using amplitude-adjusted plane-wave destruction filters. Plane-wave destruction can efficiently measure shifts of less than a few samples, making this algorithm particularly effective for detecting small shifts. Separating shifts and scales allows shifting functions to be measured more accurately. When shifts are large, amplitude-adjusted plane-wave destruction can also be used to refine shift estimates obtained by other methods. The effectiveness of this algorithm in predicting shifting and scaling functions is demonstrated by applying it to a synthetic trace, a time-lapse field data set from the Cranfield CO_2 sequestration project and a multicomponent field data set from West Texas.

INTRODUCTION

Over the past 25 years, time-lapse seismic monitoring has evolved into the standard method to detect spatial fluid changes in the subsurface (Lumley, 2001). In some locations, permanent stations have been installed for continuous time-lapse monitoring (Berron et al., 2015).

Simple crosscorrelation based algorithms are among the most commonly used methods for estimating 4D timeshifts. Rickett and Lumley (2001) propose cross-

equalization, which includes spatial and temporal registration to compensate for different acquisition geometries and amplitude balancing to scale the data to the same amplitude. Fomel and Jin (2009) estimate 4D timeshifts by picking a regularized warping path which maximizes the local similarity attribute (Fomel, 2007a). Karimi et al. (2016) use the local similarity attribute to estimate 4D timeshifts after flattening the time-lapse seismic images using the stratigraphic coordinates transformation (Karimi and Fomel, 2015). Dynamic time warping (Sakoe and Chiba, 1978) was originally proposed for speech recognition and has been applied to estimating 4D timeshifts and many other data registration problems in geophysics (Hale, 2013a). Williamson et al. (2007) explain timeshifts and amplitude changes by integrating classical warping and impedance inversion in the limit of small offset and dip and low frequency. This method is particularly attractive, as it iteratively compensates for amplitude changes associated with velocity variations induced by fluid injection or production. Hoeber et al. (2008) incorporate complex trace analysis (Taner et al., 1979) to match local phase and amplitudes between time-lapse seismic images. Lie (2011) extracts both timeshifts and 4D signal using a constrained inversion scheme. Zhang and Du (2016) borrow the optical flow technique (Horn and Schunck, 1981) to predict multidimensional timeshifts at multiple scales.

In this thesis, I adopt and extend plane-wave destruction (Fomel, 2002; Chen et al., 2013a) for automatic estimation of time-variant shifts and rescaling functions between seismic images. This technique iteratively refines timeshift estimates by predicting amplitude changes from the seismic data. In time-lapse seismic monitoring, sensitive acquisition and processing is required to detect small shifts induced by fluid migration. I show that the proposed amplitude-adjusted plane-wave destruction filters are particularly effective in measuring small shifts and test the proposed algorithm

using synthetic and field data examples.

Multicomponent receivers and SH sources allow S-waves to be processed along with P waves to create multiple images of the subsurface. Similarly to time-lapse images, multicomponent images must be registered to the same frame of reference for proper interpretation (Hardage et al., 2011). In multicomponent image registration, it is important to measure shifts to high resolution to ensure that the images are in the same reference frame.

THEORY

In the application of estimating timeshifts between time-lapse and multicomponent seismic images, I modify the amplitude-adjusted plane-wave destruction filter to

$$C(a, p, Z_1, Z_4) = B(p, Z_1^{-1}) - aZ_4B(p, Z_1) \ , \tag{3.1}$$

where Z_4 represents a shift between images. The objective of this filter remains the same – to minimize the plane-wave residual. In the time-lapse application, I scale and warp the monitor image to match the baseline image. In the multicomponent application I scale and warp one component to match another. Timeshifts between vertical-horizontal or horizontal-horizontal can be used to characterize subsurface fractures.

This algorithm efficiently matches images by estimating shifting and scaling functions. The estimated shifts and scaling weights are constrained to be smooth using shaping regularization (Fomel, 2007b).

SYNTHETIC EXAMPLE

I first test the proposed algorithm by generating a random synthetic base trace, shifting function, and scaling function (Figure 3.1(a)). The warping and scaling functions are applied to the base trace to create a synthetic monitor trace. I attempt to measure the shifting and scaling functions from the synthetic base and monitor traces using the proposed algorithm and compare the results with those from alternative algorithms.

I first apply the dynamic time warping algorithm (Sakoe and Chiba, 1978; Herrera and van der Baan, 2012; Hale, 2013b). This algorithm is particularly effective when measuring large shifts, but it only computes integer shifts between samples on a predefined grid. In this synthetic example and many real examples from time-lapse monitoring, shifts are quite small and dynamic time warping is not always effective. Indeed, the shifting function measured with dynamic time warping does not effectively measure the small shifts in the synthetic trace and contains the unappealing "stair-stepping" artifact due to the algorithm's inability to measure shifts outside of the predefined sampling grid (Figure 3.1(a)).

I then apply the local similarity scan (Fomel, 2007b, 2009) to measure the local shifting function. This algorithm scans through shifts, computing local similarity and picking the optimal warping path automatically. In our synthetic tests, this algorithm effectively measures the low frequency component of the synthetic shifting function, but fails to detect higher-frequency variations (Figure 3.1(b)).

Finally, I measure the shift using the proposed amplitude-adjusted plane-wave destruction algorithm. Compared to dynamic time warping and local similarity, plane-wave destruction proves to be particularly effective when measuring small,

rapidly varying shifting functions. After only 5 iterations, the measured shifting function converges to the predefined synthetic shift (Figure 3.1(c)). Synthetic scaling functions are also measured effectively (Figure 3.1(d)). After applying the measured shifting and scaling functions to the synthetic monitor trace, the result is visually indistinguishable from the synthetic base trace (Figure 3.1(f)).

TIME-LAPSE DATA REGISTRATION

I then apply amplitude-adjusted plane-wave destruction to time-lapse field data from the Cranfield CO_2 sequestration experiment (Zhang et al., 2013, 2014). This data set consists of a base (Figure 3.2) and monitor (Figure 3.3) image.

Plane-wave destruction is particularly effective for measuring very small shifts. Furthermore, rescaling the monitor image to match the amplitude of the base images allows local shifts to be measured even more precisely. Upon applying the algorithm, high resolution shifting (Figure 3.4) and scaling (Figure 3.5) functions are computed and applied to the previously shifted image to improve the match between the base and monitor image.

To display the results, I interleave a slice of the base cube with slices of the unaltered monitor cube (Figure 3.13(a)) and the shifted monitor cube (Figure 3.13(a)) and see that reflections become aligned effectively after applying the proposed algorithm, indicating that the shifting and scaling functions have been properly predicted.

I finally compute the time-lapse difference (Figure 3.7) and the registered difference (Figure 3.8). Coherent signal can be interpreted throughout the time-lapse difference due to the timeshift between the images. Upon registering the images, the difference outside of the reservoir interval reduces to noise. The signal between 2.2

and 2.3 s corresponds to the reservoir where CO_2 injection took place between the surveys.

MULTICOMPONENT DATA REGISTRATION

Next, I apply amplitude-adjusted plane-wave destruction filters to a multicomponent field data example from a carbonate field in West Texas.

This example consists of two PS images from different horizontal components. Events in one image are consistently faster than the other due to anisotropic effects associated with fractures (Figures 3.9 and 3.10).

I use a similarity scan to calculate an initial estimate of the shift between the fast and slow images (Figure 3.11). I subsequently apply amplitude-adjusted plane-wave destruction filters to estimate the time-shift to higher resolution. Plane-wave destruction is particularly effective for measuring very small shifts. Furthermore, rescaling the the slow image to match the amplitude of the fast image allows local shifts to be measured more precisely. Upon applying the algorithm, high resolution shifting and scaling functions are computed and applied to the previously shifted image to improve the correlation between the fast and slow PS image (Figure 3.12).

To visualize the effectiveness of local similarity and amplitude-adjusted plane-wave destruction filters in estimating time-shifts between PS fast and slow images, I interleave the images before registration (Figure 3.13(a)), after registration using timeshifts estimated using the local similarity attribute (Figure 3.13(b)), and after registration using amplitude-adjusted plane-wave destruction filters (Figure 3.13(c)). After registering the images, the reflections become aligned, indicating that the time-shifts have been estimated properly.

DISCUSSION AND CONCLUSIONS

The proposed amplitude-adjusted plane-wave destruction algorithm provides high resolution scaling and vertical shifting functions to be computed between time-lapse seismic images. Accurate prediction of time-lapse timeshifts is important for monitoring fluid migration and reservoir compaction (Hatchell and Bourne, 2005). In seismic image registration, vertical shifts are sometimes insufficient for matching the images. Lateral shifts may be required as well (Hale et al., 2008; Hale, 2009a; Cox and Hatchell, 2008). Multidimensional shifts may be estimated by incorporating amplitude-adjustment into omnidirectional plane-wave destruction (Chen et al., 2013b).

Furthermore, traditional time-lapse seismic image registration algorithms perform well in the absence of amplitude changes between baseline and monitor images. This assumption generally fails at the reservoir level where fluid injection and/or production induce changes in the elastic and sonic properties of the interval. These changing amplitudes can produce spurious timeshift anomalies (MacBeth et al., 2016). This effect is most pronounced near the tuning thickness due to interference between reflection events associated with thin beds. Similarly, low frequencies can produce arbitrarily large timeshifts. Phillips and Fomel (2017a) proposes an extension of this algorithm to estimate timeshifts in the presence of these problematic amplitude changes by decomposing time-lapse images into discrete frequencies components and simultaneously inverting for regularized timeshifts and amplitude ratios between baseline and monitor seismic images.

The proposed algorithm utilizes a modification of plane-wave destruction filters to acquire high-resolution shifting and scaling functions between monitor images and

a base image. Plane-wave destruction is particularly effective for measuring small shifts. When shifts are small, amplitude-adjusted plane-wave destruction can be used as a standalone algorithm to efficiently measure shifting and scaling functions between seismic images. When shifts are large, the proposed algorithm can be used to refine shift predictions from other registration algorithms. Separating scaling and shifting allows local shifts to be measured more precisely. The proposed algorithm has immediate applications to time-lapse and multicomponent seismic analysis (as demonstrated), as well as automatic gather flattening, legacy image merging, and automatic seismic-well ties.

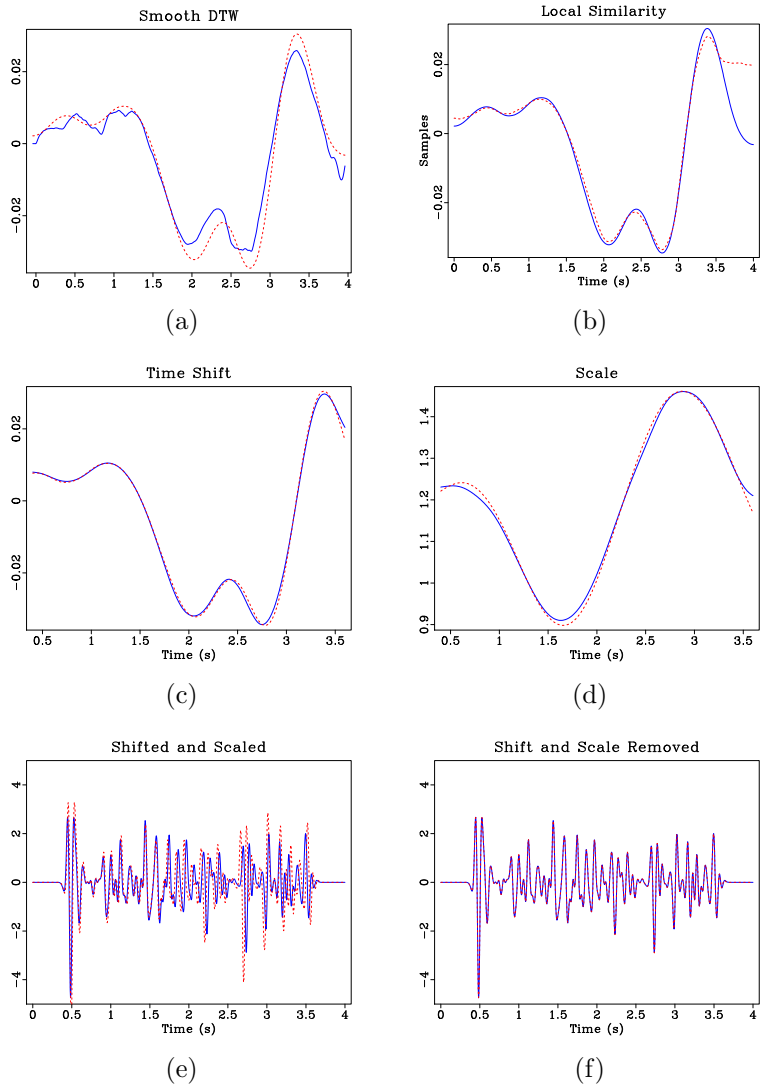

Figure 3.1: (a-c) Exact shift (dashed) and measured shift (solid) using: (a) dynamic time warping, (b) local similarity scanning, and (c) amplitude-adjusted plane-wave destruction. (d) Exact scaling function (solid) and measured scaling function using amplitude-adjusted plane-wave destruction (dashed), (e) synthetic base trace (dashed) and monitor trace (solid), and (f) synthetic base trace (dashed) and shifted and scaled monitor trace (solid) using shifting and scaling functions measured by amplitude-adjusted plane-wave destruction. ch03-regis/synth cdtwshift,lsshift,dip,a,traces,reg

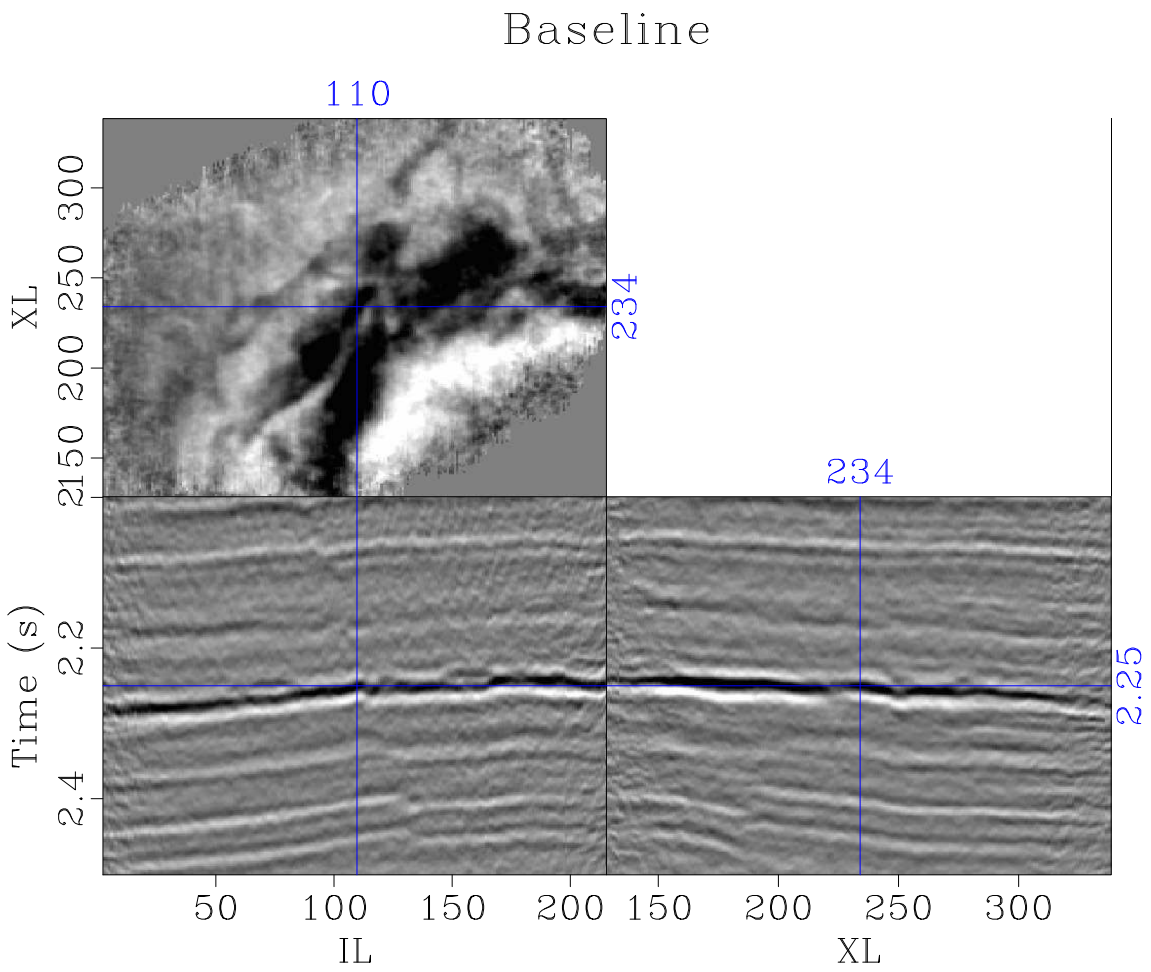

Figure 3.2: A subset of the baseline seismic image from the Cranfield CO_2 injection experiment. ch03-regis/cran baseline3

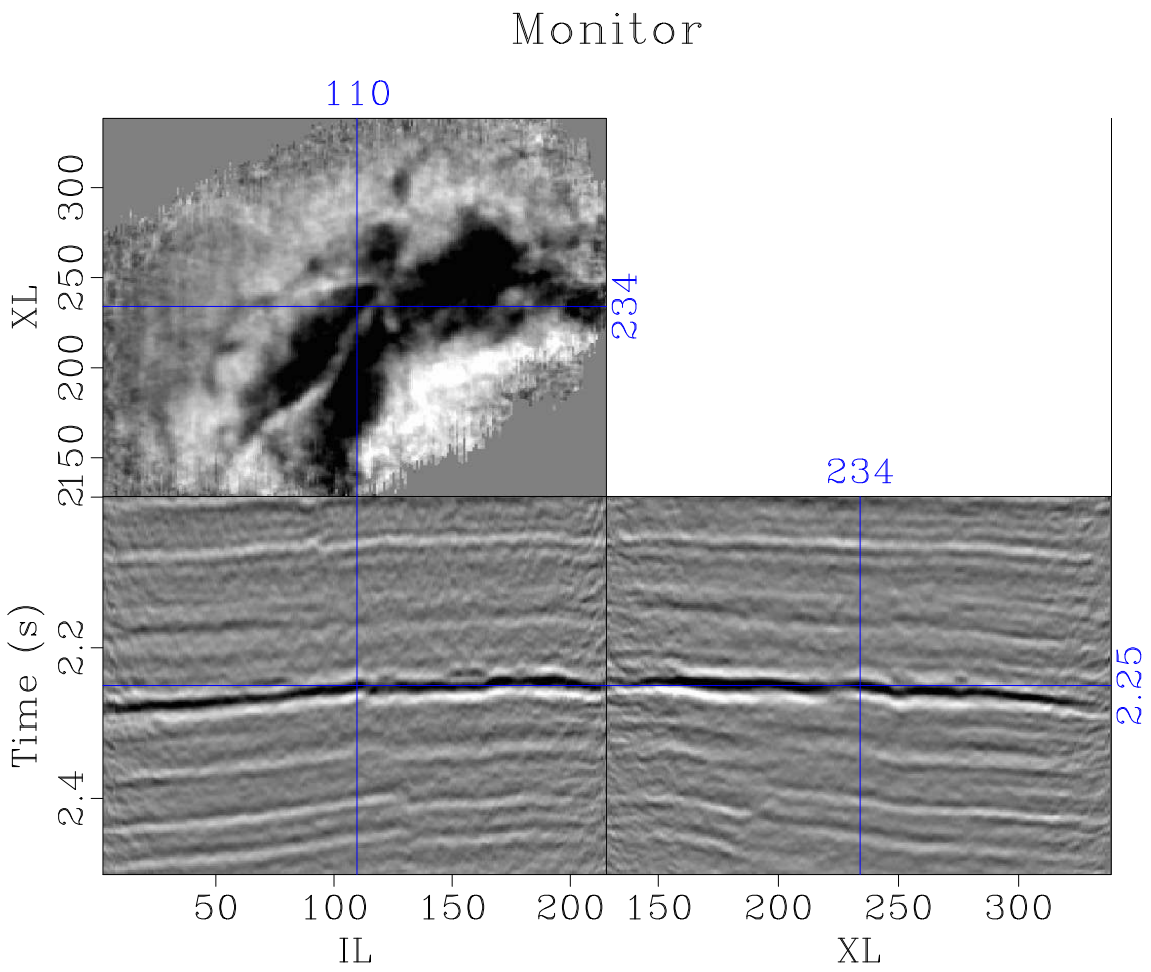

Figure 3.3: A subset of the monitor seismic image from the Cranfield CO_2 injection experiment. The injection interval is the bright reflection at approximately 2.2 - 2.3 s. ch03-regis/cran monitor3

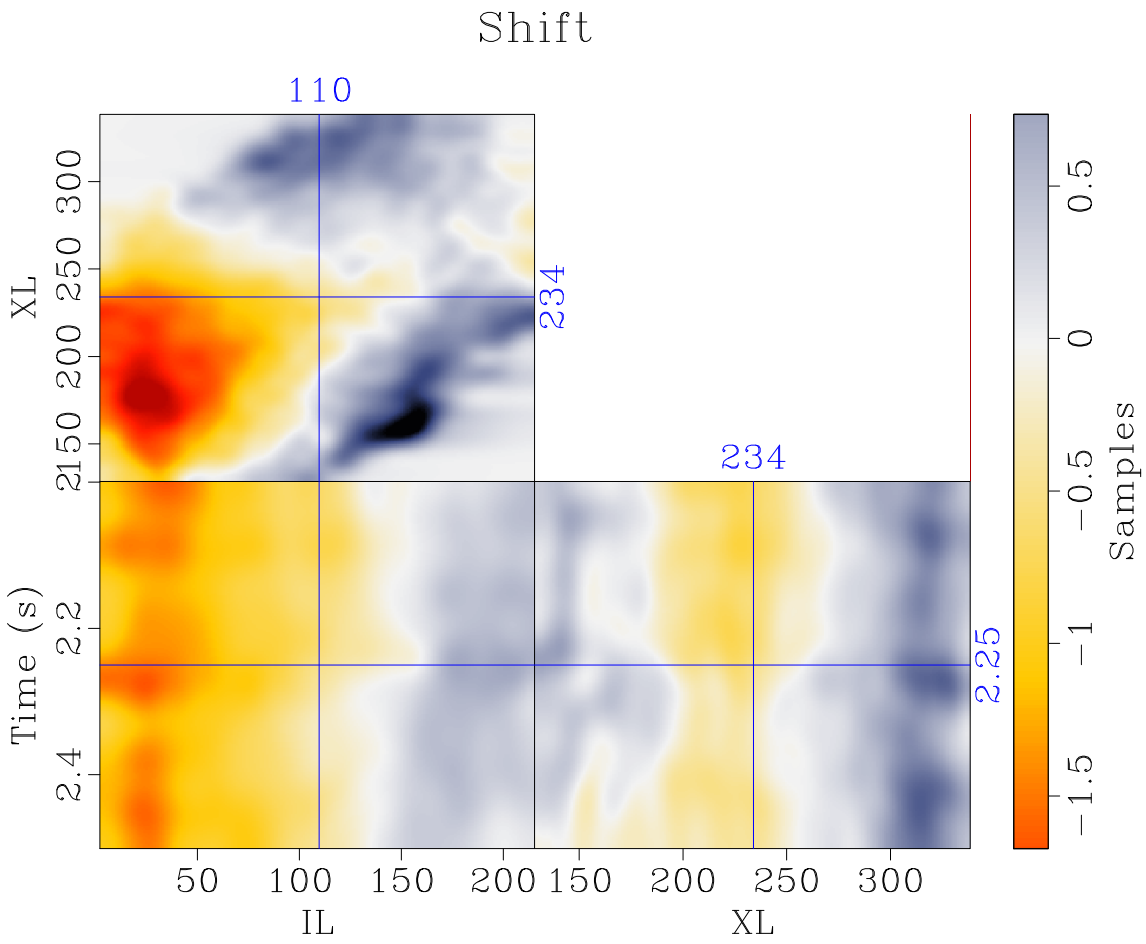

Figure 3.4: The time-shift estimated using amplitude-adjusted plane-wave destruction
ch03-regis/cran dip5

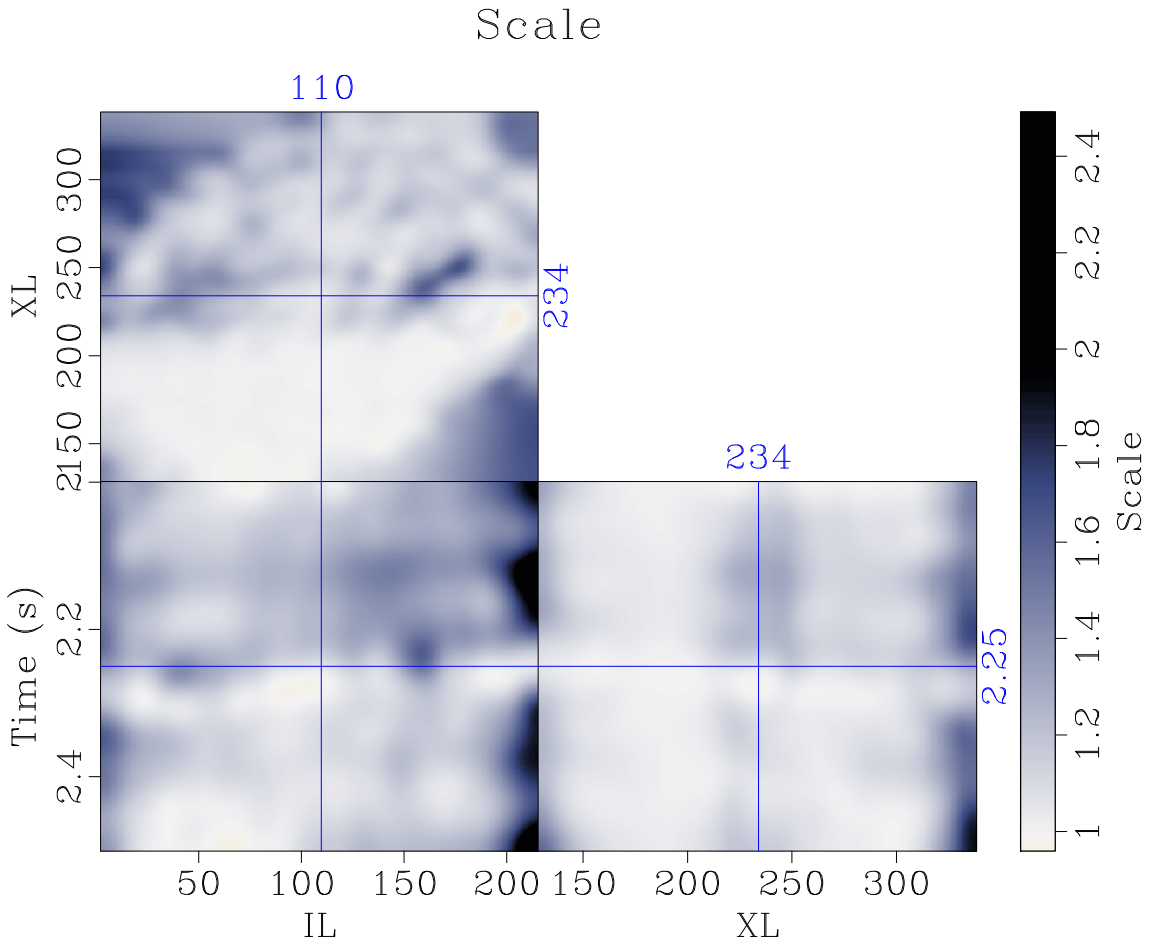

Figure 3.5: The amplitude weight estimated using amplitude-adjusted plane-wave destruction ch03-regis/cran a5

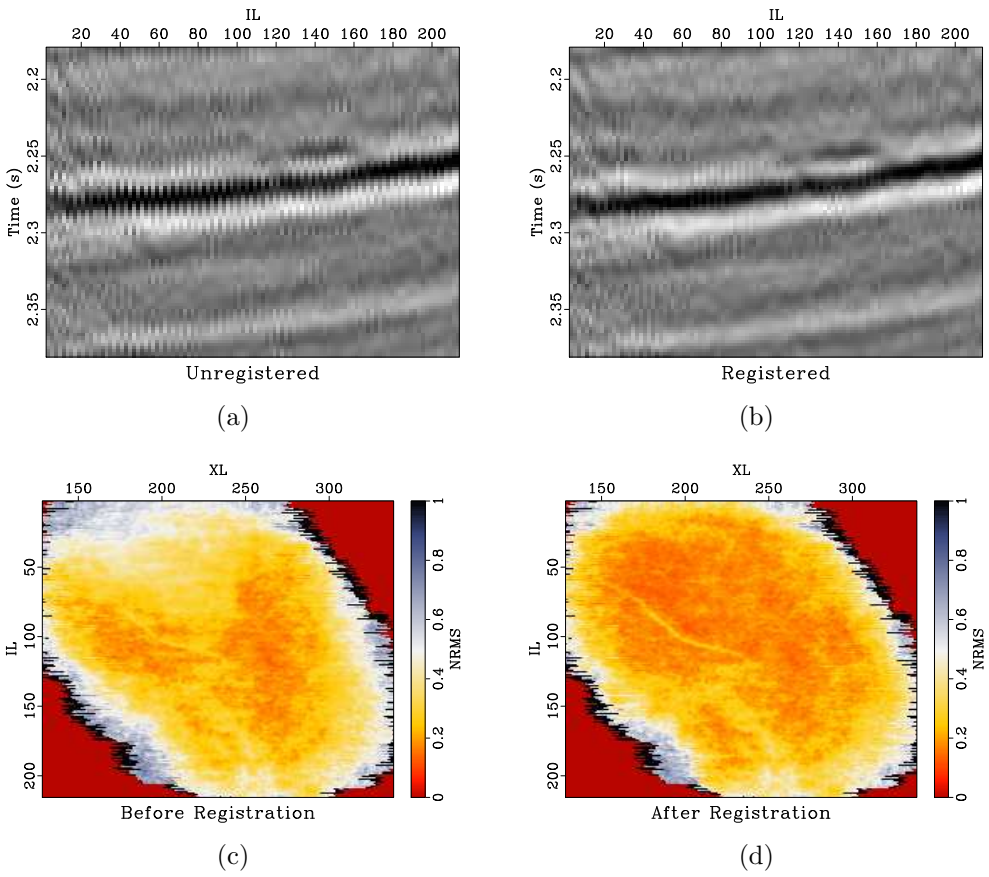

Figure 3.6: (a-b) The base image interleaved with the (a) monitor image and (b) registered monitor image and (c-d) NRMS maps between the baseline image and (c) the monitor image and (d) the registered monitor image. ch03-regis/cran int1,int2,nrms1,nrms2

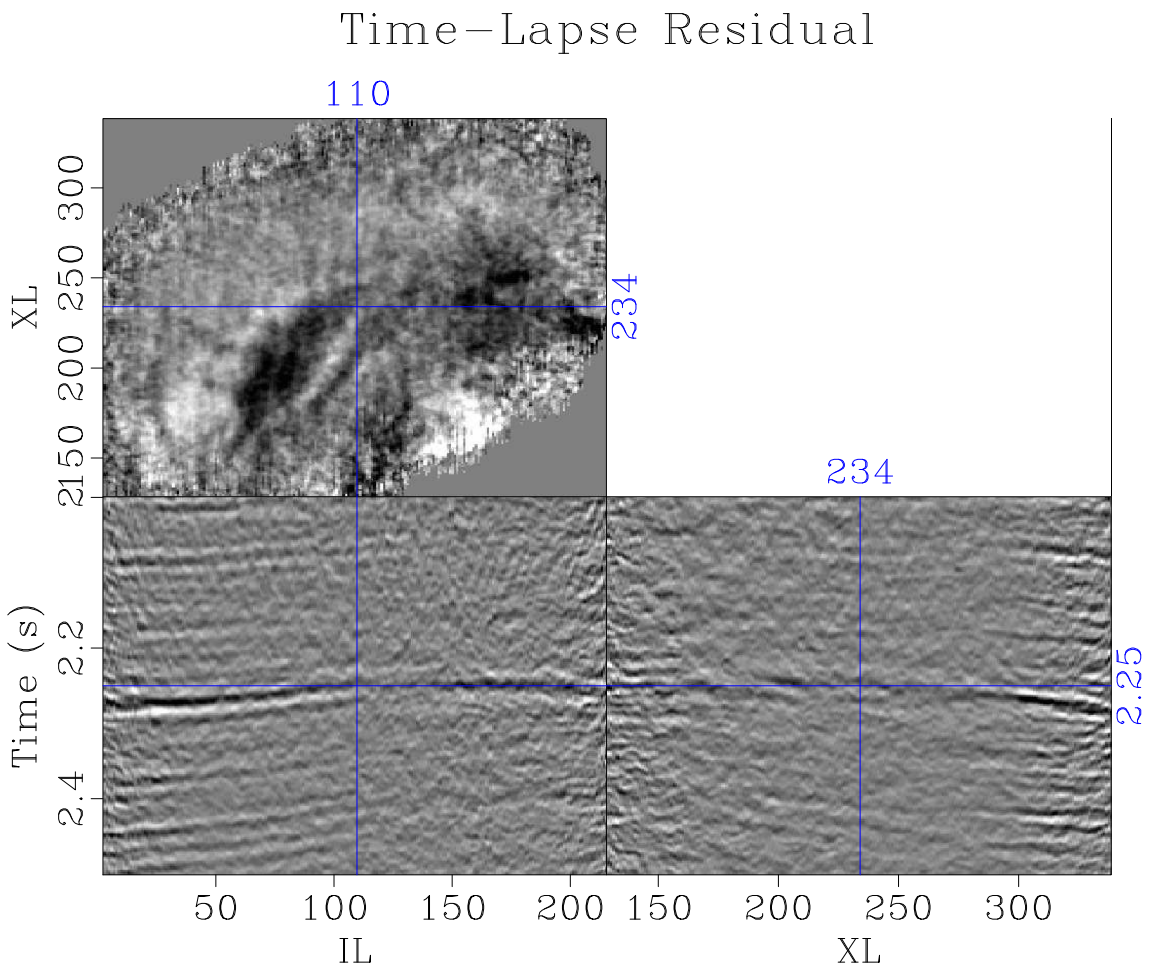

Figure 3.7: Time-lapse residual between the baseline and monitor seismic images. ch03-regis/cran res1

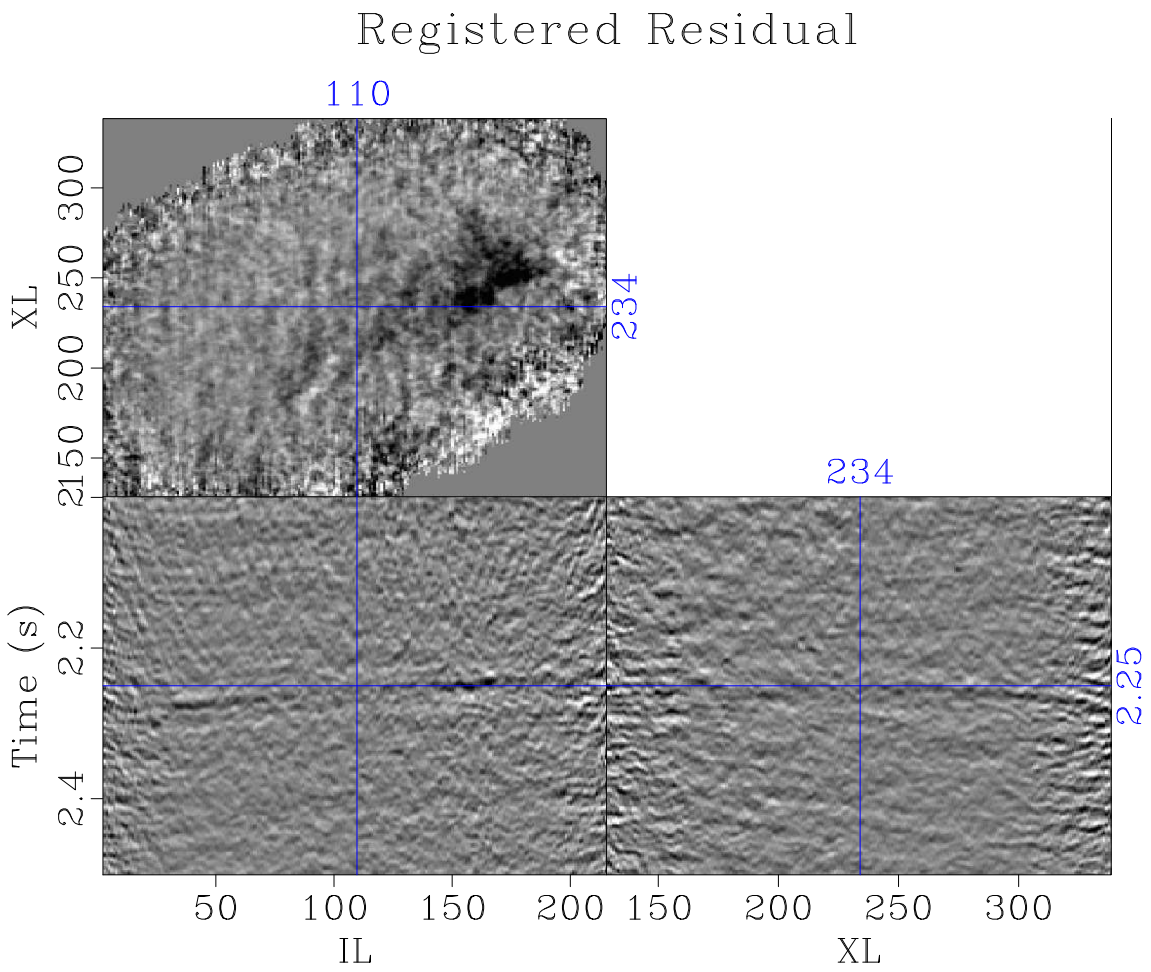

Figure 3.8: Time-lapse residual between the baseline and registered monitor seismic images. ch03-regis/cran res2

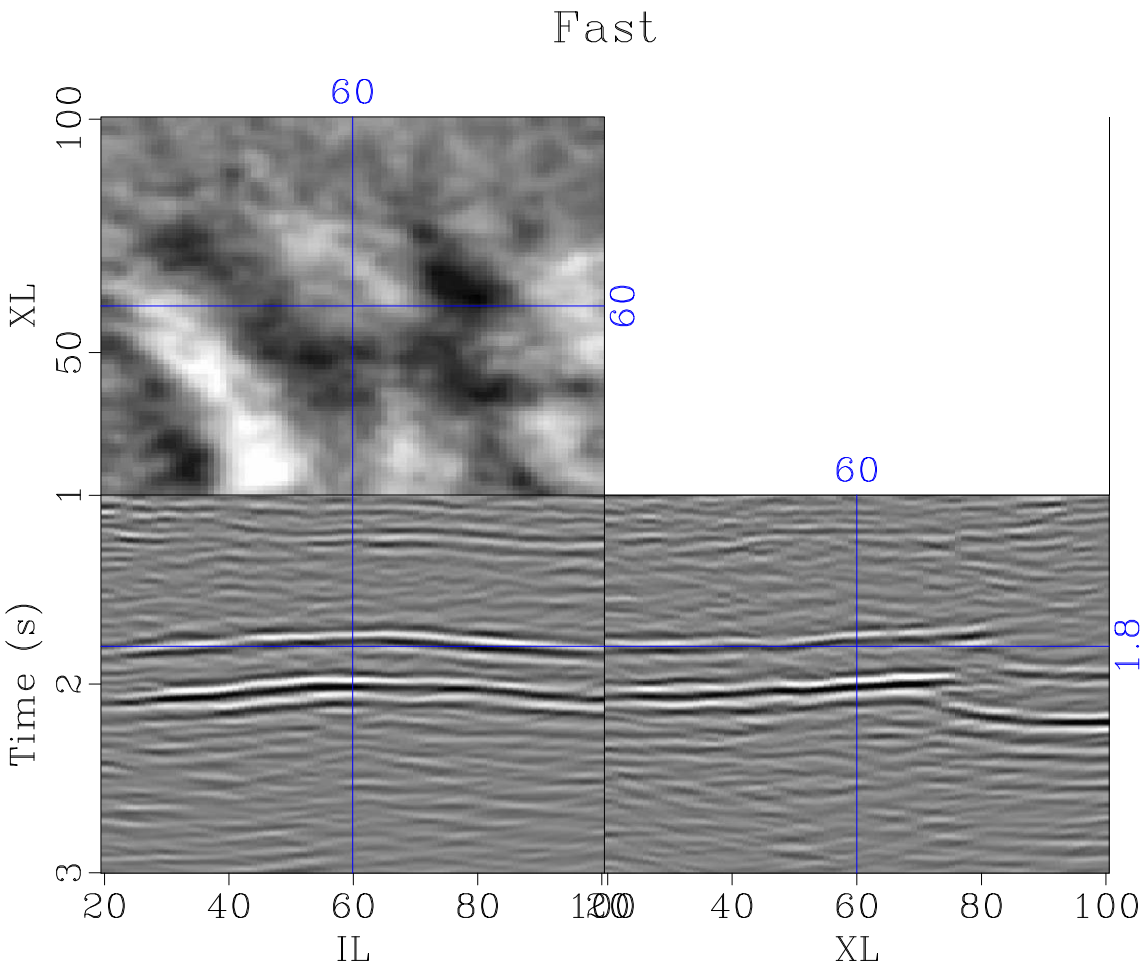

Figure 3.9: PS Fast image ch03-regis/hark Fast

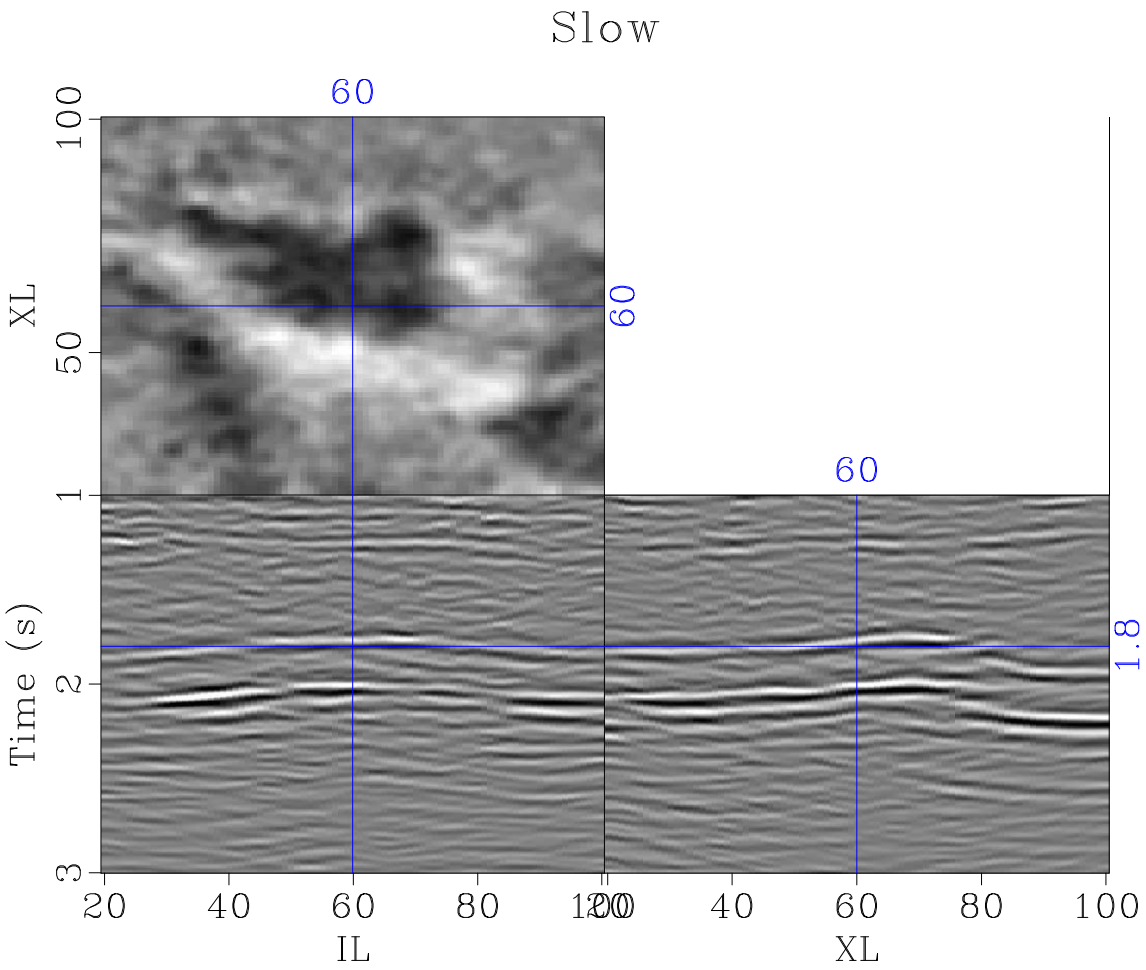

Figure 3.10: PS Slow image ch03-regis/hark Slow

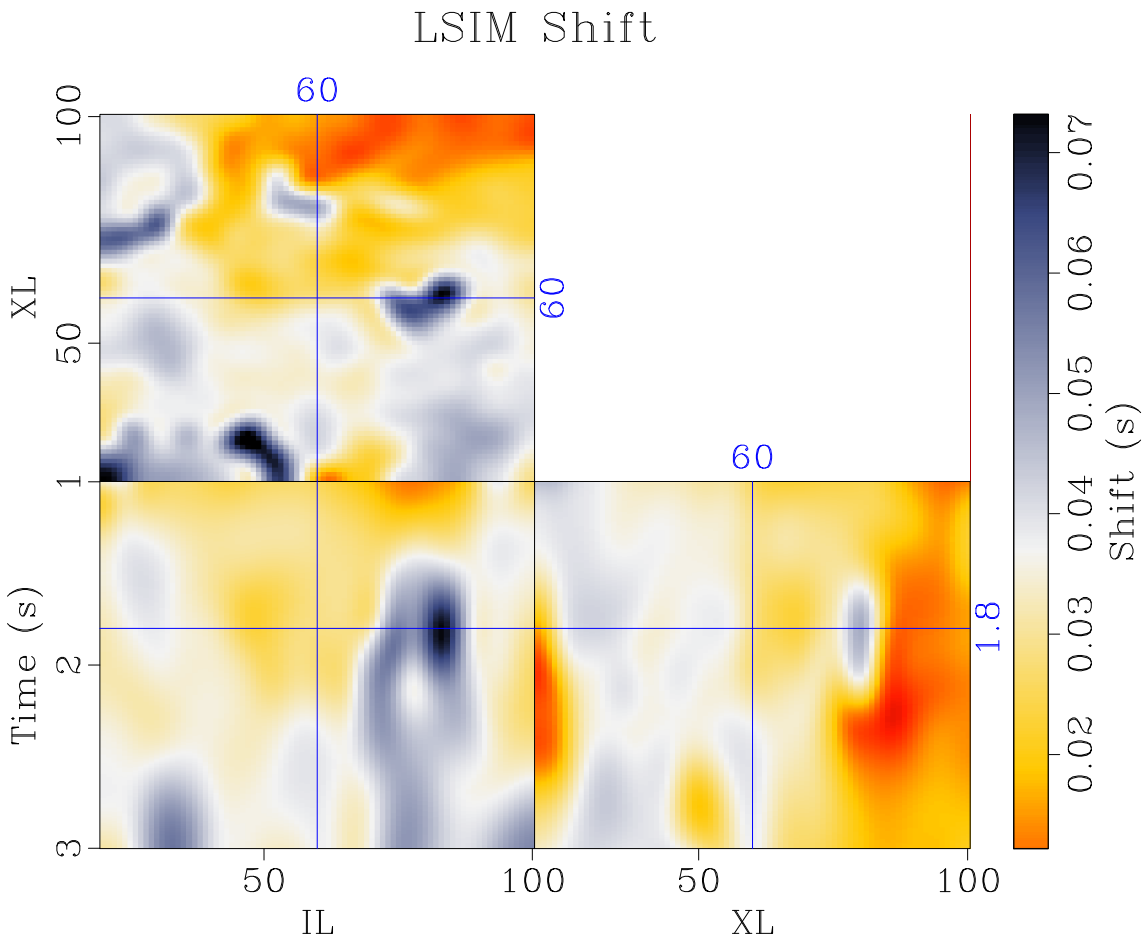

Figure 3.11: Time-shift between PS images estimated using the local similarity attribute. ch03-regis/hark pick

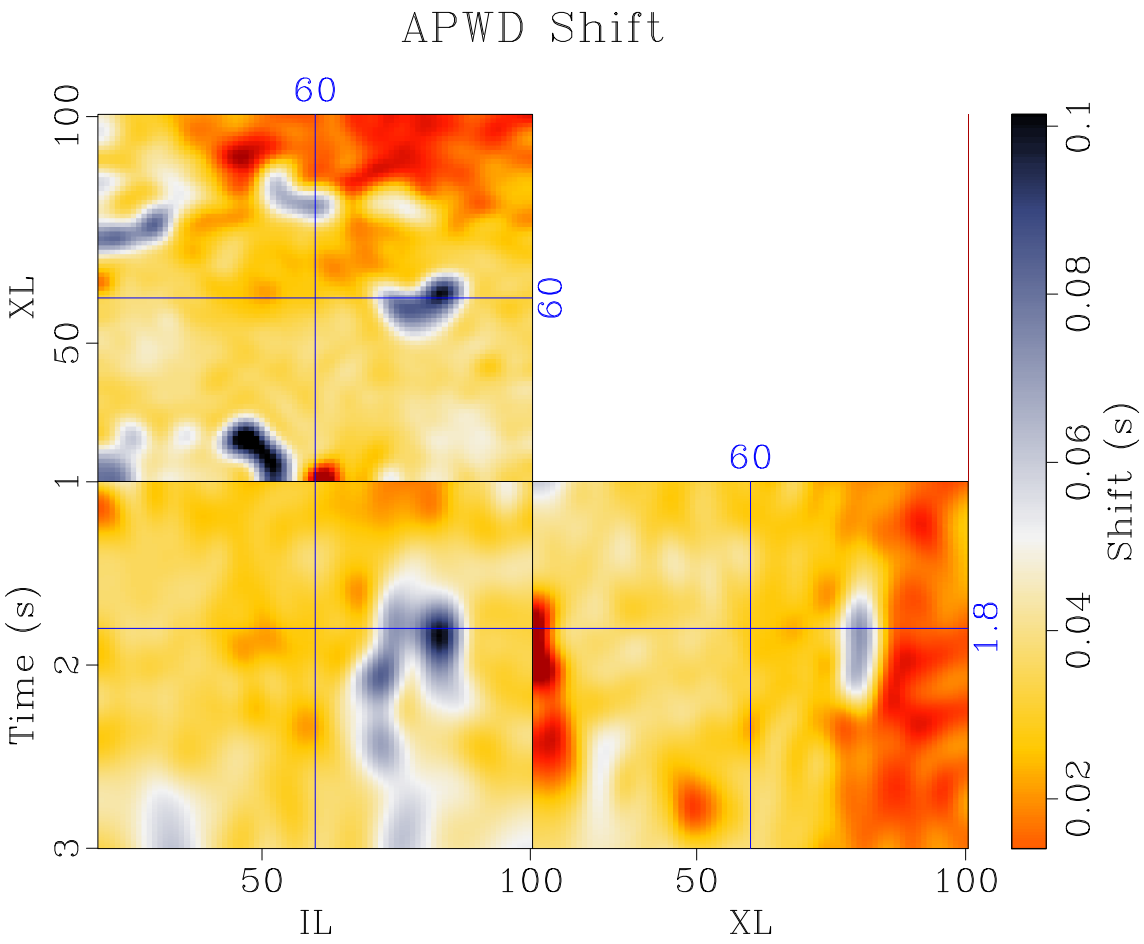

Figure 3.12: Time-shift between PS images estimated using amplitude-adjusted plane-wave destruction filters ch03-regis/hark shift

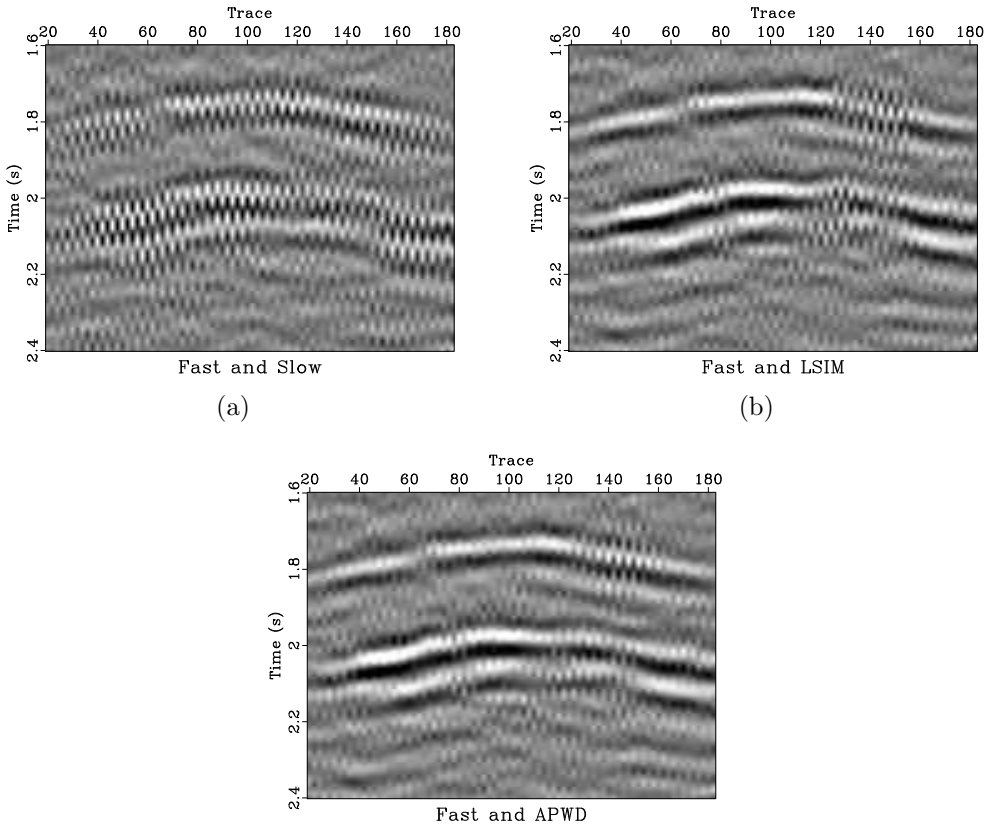

Figure 3.13: PS images interleaved (a) before and (b-c) after registration using the (b) local similarity attribute and (c) amplitude-adjusted plane-wave destruction filters. ch03-regis/hark int1,int2,int3

Chapter 4

Automatic gather flattening for AVO analysis using amplitude-adjusted plane-wave destruction

I propose a method to efficiently measure regularized residual non-hyperbolic moveout from seismic offset or angle gathers using amplitude-adjusted plane-wave destruction filters. Plane-wave destruction can efficiently measure shifts of less than a few samples, making this algorithm particularly effective for detecting small timeshifts between seismic traces. Separating estimation of timeshifts and amplitude variations allows residual non-hyperbolic moveout to be measured more accurately in the presence of AVO (amplitude variation with offset). The effectiveness of this algorithm in predicting residual moveout is demonstrated by applying it to a synthetic CMP gather and the Mobil AVO seismic data.

INTRODUCTION

Prestack seismic data is routinely flattened using moveout corrections; however, it is still difficult to eliminate all reflection curvature while maintaining a physically reasonable models of subsurface anisotropy and velocity. Flat gathers also dramatically simplify the extraction of amplitude attributes for AVO analysis.

Hinkley et al. (2004) propose to calculate offset-dependent timeshifts required to flatten all events within a gather simultaneously by crosscorrelating traces within a small 2D window. Crosscorrelations are computed between each pair of traces in

the window, building a linear system which can be solved by least-squares inversion. Gulunay et al. (2008) modifies this algorithm by tracking events using a climbing correlation window and rejecting and replacing timeshifts associated with low correlations.

Qian et al. (2016) propose to use dynamic time warping (Sakoe and Chiba, 1978; Hale, 2013a) to flatten gathers rather than crosscorrelation. Both crosscorrelation and dynamic time warping perform comparatively well when shifts are large and rapidly varying; however, in the application of automatic gather flattening, timeshifts associated with residual moveout between neighboring traces are generally quite small and such algorithms are not always effective.

Zhang and Du (2016) apply the Multi-Scale and Iterative Refinement Optical Flow (MSIROP) technique (Horn and Schunck, 1981) to seismic data registration problems, including gather flattening. This method provides a stable estimate of multidimensional timeshifts required to residually flatten image gathers. It also avoids the common cycle-skipping problem in data registration and is effective for estimating both small and large timeshifts.

None of the algorithms described above explicitly address amplitude variations as a function of offset or angle in the estimation of residual moveout corrections. In this chapter, I propose to adopt amplitude-adjusted plane-wave destruction filters, as described in chapter 2, to simultaneously estimate regularized timeshifts associated with residual non-hyperbolic moveout and amplitude variations with angle or offset. The method is capable of flattening gathers in the presence of noise, class II AVO anomalies, and anisotropy.

THEORY

Automatic gather flattening can be described as offset gather registration and falls into the same category of problems as image registration. I propose to estimate residual non-hyperbolic moveout corrections using amplitude-adjusted plane-wave destruction filters. When applied to gathers, amplitude-adjusted plane-wave destruction filters estimate dynamic timeshifts between seismic traces which correspond to non-hyperbolic moveout corrections associated with uncertainty in the velocity and anisotropy models. I specify the definition of amplitude-adjusted plane-wave destruction filters in equation 2.14 to

$$D(a, p, Z_t, Z_x) = B(p, Z_t^{-1}) - aZ_xB(p, Z_t) \ , \tag{4.1}$$

where Z_t and Z_x represent phase shifts in time and offset or angle, respectively. The objective of this filter remains the same - to minimize the plane-wave residual. The gather flattening application, I accumulate timeshifts and amplitude weights by minimizing the plane-wave residual between neighboring traces and perturbing the warping function with each offset step.

Automatic gather flattening was proposed mainly to improve the reliability and efficiency of AVO analysis, yet previously proposed algorithms can be sensitive to amplitude variations with angle or offset, particularly class II AVO anomalies. Amplitude-adjusted plane-wave destruction filters are particularly effective in this application because they simultaneously provide regularized (Fomel, 2007b) estimates of residual moveout and amplitude variations with angle or offset.

EXAMPLE I

I first test the proposed automatic gather flattening algorithm using amplitude-adjusted plane-wave destruction filters on a synthetic CMP gather with random noise, velocity variations with depth, multiples, TI anisotropy (Alkhalifah and Tsvankin, 1995), and two reservoirs with class II AVO anomalies (Castagna et al., 1998) (Figure 4.1).

Fomel (2009) proposed the AB semblance attribute, which is suitable for velocity analysis of prestack seismic data with amplitude variations with offset. This attribute can yield a good estimate of the subsurface velocity structure in the absence of anisotropy.

When amplitude-adjusted plane-wave destruction filters are applied to gathers to account for residual curvature of seismic reflection energy, it is important to remove multiple reflection energy while preserving seismic amplitudes. Multiples interfere with local slope calculation due to the presence of conflicting steep slopes. These steeply dipping events are effectively predicted and subtracted using the surface-related multiple elimination method (Verschuur et al., 1992) (Figure 4.1).

Amplitude-adjusted plane-wave destruction filters are subsequently applied to residually flatten NMO-corrected gathers and correct for non-hyperbolic moveout associated with anisotropy (Figure 4.2). The gather is residually flattened, even in the presence of noise, anisotropy, and class II AVO anomalies (Figure 4.1).

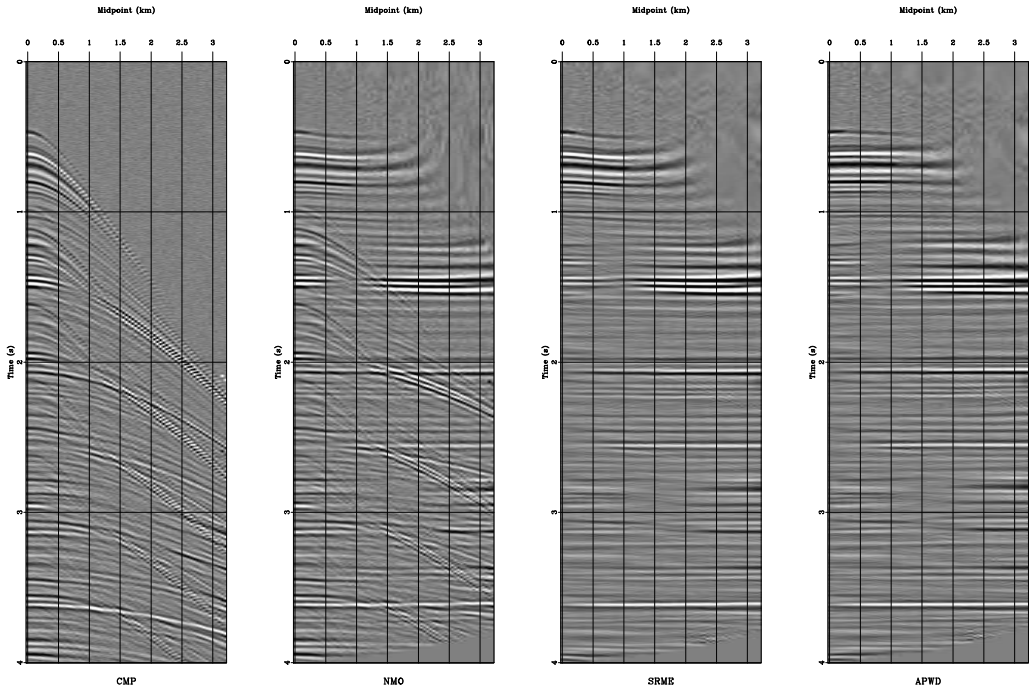

Figure 4.1: (a) Synthetic CMP gather with noise, velocity variations with depth, multiples, anisotropy, and two reservoirs with class II AVO anomalies, (b) NMO-corrected gather, (c) isolated primary reflections, and (d) residually flattened gather using amplitude-adjusted plane-wave destruction filters. ch04-agf/synth flat1

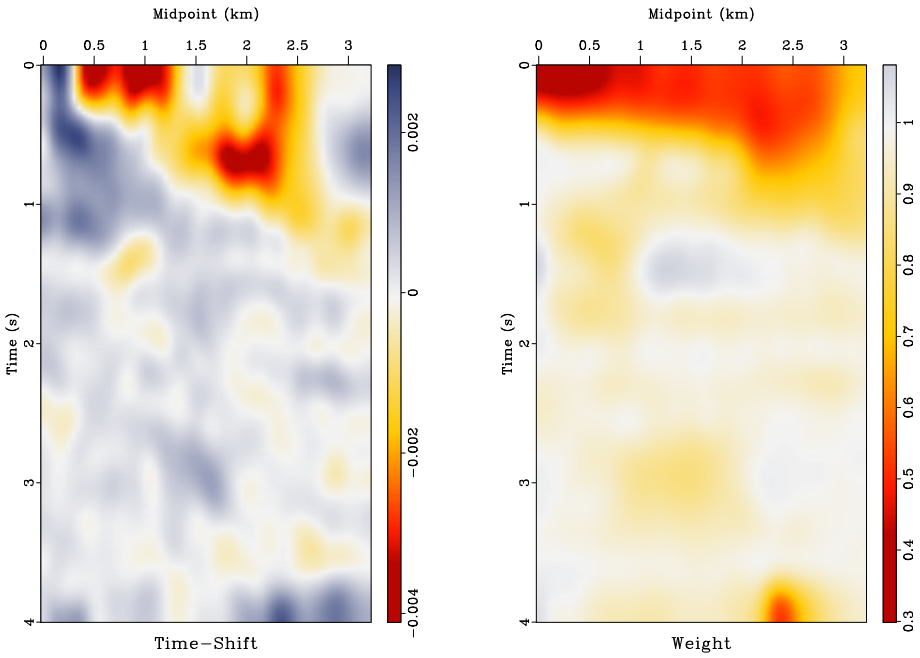

Figure 4.2: (a) Timeshifts and (b) amplitude weights predicted using amplitude-adjusted plane-wave destruction filters. ch04-agf/synth apwd1

EXAMPLE II

Amplitude-adjusted plane-wave destruction filters are next tested on the Mobil AVO prestack-stack seismic data. This 25 km 2D marine seismic line was acquired by Mobil Oil in the Viking Graben, North Sea, and has been widely used to validate AVO and multiple attenuation algorithms (Keys and Foster, 1998). The data set is available in the SEG open data repository (`http://wiki.seg.org/wiki/Mobil_AVO_viking_graben_line_12`).

The data is preprocessed in the shot domain, including deconvolution with the far field wavelet, hyperbolic muting of the direct-wave and diving waves, spherical divergence corrections (Fowler and Claerbout, 1983), and surface-consistent amplitude normalization (Taner and Koehler, 1981). The shots are transformed to the CMP domain and the same workflow applied in the synthetic case is applied to the field data: AVO-friendly semblance-based velocity analysis (Fomel, 2009), surface-related multiple elimination (Verschuur et al., 1992), and residual gather flattening using amplitude-adjusted plane-wave destruction filters (Figure 4.3). The workflow described automatically flattens gathers, improving the reliability of automatic AVO interpretation from prestack seismic data.

CONCLUSIONS

Amplitude-adjusted plane-wave destruction filters provide an estimate of regularized residual non-hyperbolic moveout when applied to gathers. Because plane-wave destruction is particularly effective for measuring small shifts, when residual moveout corrections are relatively small, amplitude-adjusted plane-wave destruction can be used to efficiently and automatically flatten gathers for AVO analysis. Separating

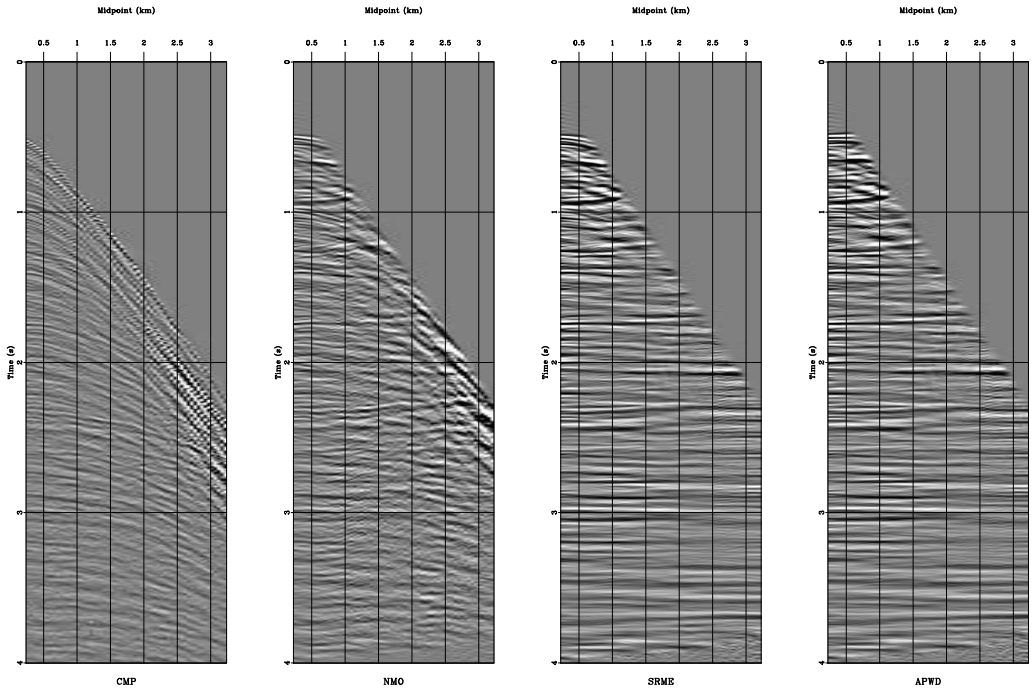

Figure 4.3: (a) Mobil AVO CMP gather # 1201, (b) NMO-corrected gather, (c) isolated primary reflections, and (d) residually flattened gather using amplitude-adjusted plane-wave destruction filters. ch04-agf/vik flat2

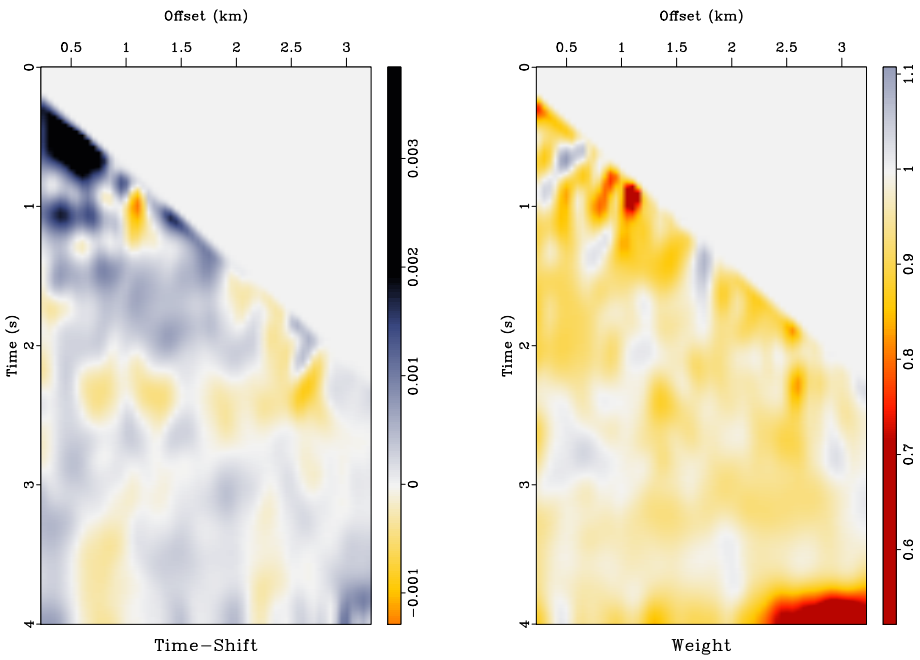

Figure 4.4: (a) Timeshifts and (b) amplitude weights predicted using amplitude-adjusted plane-wave destruction filters. ch04-agf/vik apwd2

the computation of residual moveout and amplitude variations allow each term to be measured more precisely.

Chapter 5

Plane-wave Sobel attribute for discontinuity enhancement in seismic images

Discontinuity enhancement attributes are commonly used to facilitate the interpretation process by enhancing edges in seismic images and providing a quantitative measure of the significance of discontinuous features. These attributes require careful pre-processing to maintain geologic features and suppress acquisition and processing artifacts which may be artificially detected as a geologic edge.

I propose the plane-wave Sobel attribute, a modification of the classic Sobel filter, by orienting the filter along seismic structures using plane-wave destruction and plane-wave shaping. The plane-wave Sobel attribute can be applied directly to a seismic image to efficiently and effectively enhance discontinuous features, or to a coherence image to create a sharper and more detailed image. Two field benchmark data sets with many faults and channel features from offshore New Zealand and offshore Nova Scotia demonstrate the effectiveness of this method in comparison with conventional coherence attributes.

One of the major challenges of interpreting seismic images is the delineation of reflection discontinuities that are related to distinct geologic features, such as faults, channels, salt boundaries, and unconformities. Visually prominent reflection features often overshadow these subtle discontinuous features which are critical to understanding the structural and depositional environment of the subsurface. For this reason,

precise manual interpretation of these reflection discontinuities in seismic images can be tedious and time-consuming, especially when data quality is poor. Discontinuity enhancement attributes are among the most widely used seismic attributes today. These attributes are generally post-stack image domain calculations of the similarity or dissimilarity along a horizon or time slice between a neighborhood of adjacent seismic traces (Barnes, 2016). Discontinuous features, such as faults, channels, salt boundaries, unconformities, mass-transport complexes, and subtle stratigraphic features can be identified as areas of low similarity. Such attributes are powerful interpretation tools that enable detailed interpretation of previously indistinguishable features.

Bahorich and Farmer (1995) proposed the first celebrated discontinuity enhancement attribute and coined the term "coherence". The attribute produces images of the normalized local cross-correlations between adjacent seismic traces and combines them to estimate coherence. This algorithm provided the framework for semblance, the generalization to an arbitrary number of traces, proposed by Marfurt et al. (1998). Using multidimensional correlations, this approach improves vertical resolution. Both of these correlation-based methods can be sensitive to lateral amplitude variations, which may obscure features such as faults and channels.

The local covariance matrix measures the uniformity of a seismic image in each dimension. Decomposing this matrix into its eigenvectors and eigenvalues provides a quantitative measure of local variations of seismic structures. Gersztenkorn and Marfurt (1999) propose to compute the ratio of the largest eigenvalue and the sum of all eigenvalues of the covariance matrix at each sample, highlighting areas where there is no dominant texture in the seismic image. This attribute is commonly called "eigenstructure coherence" and is only sensitive to lateral changes in phase. A sim-

ilar decomposition can be applied to the structure-tensor which measures the local covariance of the image in each dimension (Randen et al., 2000, 2001; Bakker, 2002). Local linearity and planarity can be computed from the eigenvalues of the structure-tensor. Wu (2017) proposes to modify the traditional structure-tensor decomposition by orienting the image gradient along seismic structures. Discontinuous features are highlighted further by smoothing along discontinuities.

Information about reflection dip in seismic images allow filters to be oriented along seismic reflections. Variance is a simple, but effective attribute which highlights unpredictable signal associated with discontinuous features. The local variance calculation is oriented along structure using the eigenvectors of the structure-tensor (Randen et al., 2001). Hale (2009b) also orients semblance along seismic reflections using the eigenvectors of the structure-tensor, and additionally applies smoothing along directions perpendicular to the reflections to provide an enhanced image. Karimi et al. (2015) uses predictive painting (Fomel, 2010) to generate multiple predictions of local structures in seismic images. The difference between the predicted and real data provides an image with isolated discontinuities.

To compute a discontinuity enhancement image for detection and extraction of fault surfaces, semblance can be computed along fault strike and dip orientations. Cohen et al. (2006) use the normalized differential entropy attribute to enhance faults. Local fault planes are separated and extracted using an adaptive image-binarization-and-skeletonization algorithm. This method effectively extracts fault surfaces by segmenting the coherence image. Hale (2013b) and Wu and Hale (2016) propose to scan through fault strikes and dips to maximize the semblance attribute. Fault surfaces are constructed by picking along the ridges of the likelihood attribute. Additionally, images can be unfaulted by estimating fault throws using correlations of seismic

reflections across fault surfaces (Wu et al., 2016).

In image analysis, the traditional Sobel filter can be used to efficiently compute an image with enhanced discontinuities (Sobel and Feldman, 1968). The Sobel filter is an edge detector which computes an approximation of the gradient of the image intensity function at each point by convolving the data with a zero-phase discrete differential operator and a perpendicular triangular smoothing filter. This 2D filter is small and integer-valued in each direction, making it computationally inexpensive to apply to images (O'Gorman et al., 2008). Luo et al. (1996) first proposed the applications of Sobel filters to seismic images. Since, modifications of the Sobel filter have been proposed for edge detection in seismic images by orienting the filter along local slopes estimated by maximizing local cross-correlation and dynamically adapting the size of the filter based on local frequency content (Aqrawi et al., 2011; Aqrawi and Boe, 2011; Aqrawi, 2014). Dip-oriented Sobel filters can be applied directly to a seismic image to compute an image with enhanced edges, or to coherence images to further sharpen previously enhanced edges (Chopra et al., 2014).

I propose to modify the definition of the Sobel filter to follow seismic structures. I modify the Sobel filter by replacing the discrete differential operator with linear plane-wave destruction (Fomel, 2002) and triangular smoothing with plane-wave shaping (Fomel, 2007b; Swindeman and Fomel, 2015; Phillips et al., 2016). This method is particularly efficient because it does not require computation of the eigenvectors of the covariance matrix or structure-tensor. Local slopes are instead estimated using accelerated plane-wave destruction (Chen et al., 2013a). I further modify the Sobel filter by orienting the filter along the azimuth perpendicular to discontinuities by implementing an azimuth scanning workflow (Merzlikin et al., 2016). This modification is tested on benchmark 3D seismic images from offshore New Zealand

and Nova Scotia, Canada and compare the results with those from alternative coherence attributes.

THEORY

I propose to modify the traditional Sobel filter for application to 3D seismic images by orienting the filter along the structure of seismic reflectors. I modify the Sobel filter by replacing the derivative operation with plane-wave destruction (Fomel, 2002) and the smoothing operation with plane-wave shaping (Fomel, 2007b; Swindeman and Fomel, 2015). High order plane-wave destruction filters are described in the Z-transform notation according to equation 2.11 as follows:

$$\begin{array}{l} C_i(p_i) = B(p_i, Z_t^{-1}) - Z_i B(p_i, Z_t) \\ C_x(p_x) = B(p_x, Z_t^{-1}) - Z_x B(p_x, Z_t) \end{array} \quad , \tag{5.1}$$

where C is the plane-wave destruction filter, B is an all-pass filter, and p_i and p_x are the local slopes in the inline and crossline directions, respectively.

Inline and crossline shaping filters are applied to the crossline and inline plane-wave destruction images, respectively. Thus, the plane-wave Sobel filter modifies equation (3) by effectively replacing Z_i with

$$Z_i \frac{B(p_i, Z_t)}{B(p_i, Z_t^{-1})} \tag{5.2}$$

and Z_x with

$$Z_x \frac{B(p_x, Z_t)}{B(p_x, Z_t^{-1})} \ . \tag{5.3}$$

This modification effectively orients the plane-wave Sobel filter along seismic reflection structures.

In the conventional implementation, the inline and crossline images are combined to produce the final image (equation 2.21). I propose an alternative approach based on the efficient azimuth scanning workflow (Merzlikin et al., 2016). I scan through a window of azimuths and compute the L_q norm of linear combinations of the inline and crossline images weighted by the sine and cosine of the azimuth α

$$\hat{\mathbf{S}}(\alpha, p_i, p_x) = \|\mathbf{S}_i(p_i, p_x)\mathbf{d}\cos\alpha + \mathbf{S}_x(p_i, p_x)\mathbf{d}\sin\alpha\|_q \ , \tag{5.4}$$

where $\mathbf{S}_i(p_i, p_x)$ and $\mathbf{S}_x(p_i, p_x)$ correspond to convolution operators with the filters $S_i(p_i, p_x)$ and $S_x(p_i, p_x)$, respectively. The azimuth which corresponds with the discontinuous features produces the best image at each point is picked on a semblance-like panel using a regularized automatic picking algorithm (Fomel, 2009). The ensemble of images is then sliced using the pick to generate the optimal image This improves the resolution of discontinuous features by effectively orienting the plane-wave Sobel filter perpendicular to edges in the seismic image.

EXAMPLE I

Our first example is a subset of the Parihaka seismic data (full-stack, anisotropic, Kirchhoff prestack time migrated). This marine 3D seismic volume was acquired offshore New Zealand and is available in the SEG open data repository (`http://wiki.seg.org/wiki/Parihaka-3D`).

This image contains complex geologic structures, including multiple generations of faulting, meandering channel systems, and prominent unconformities. Figure 5.1 shows a particularly interesting time-slice (1.311 s) containing many faults and channels.

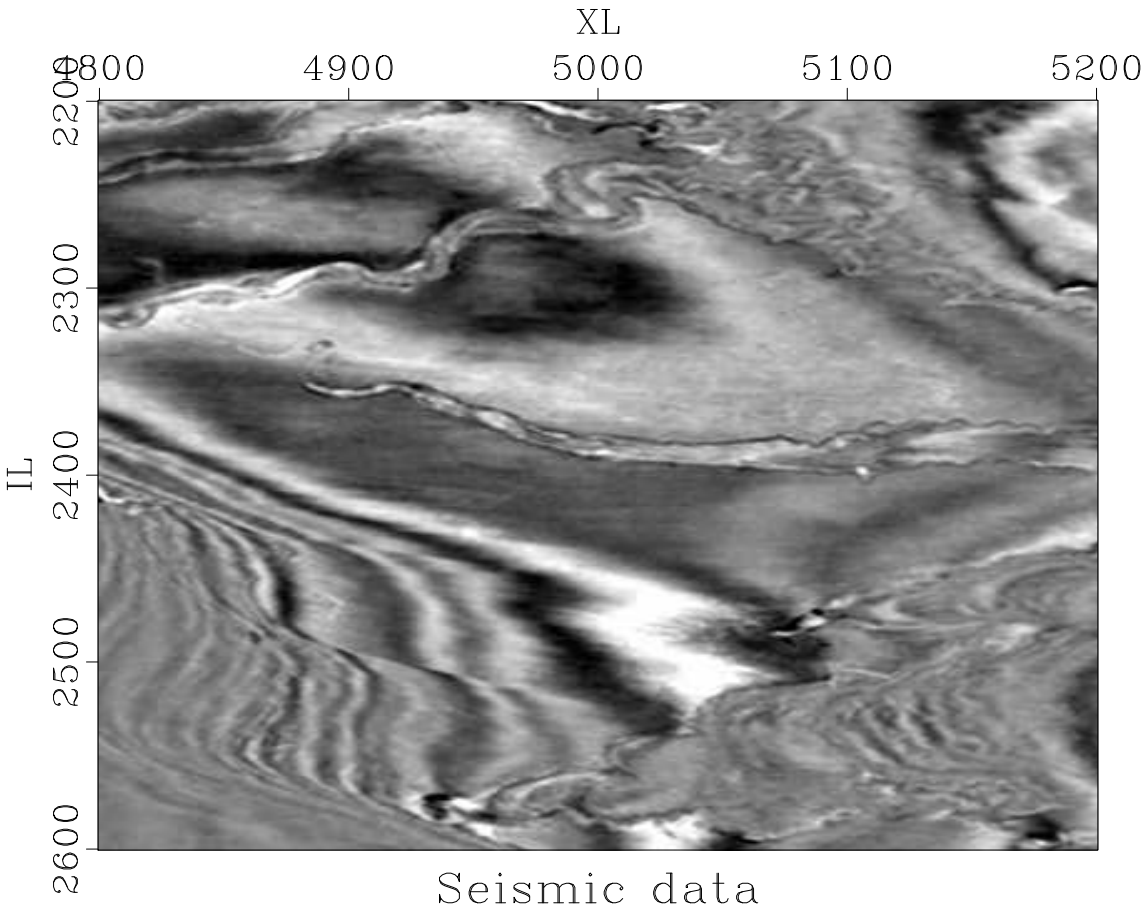

Figure 5.1: (a) The Parihaka seismic data. ch05-sobel/pari sub

I first apply the traditional Sobel filter. This attribute enhances discontinuous geologic features, but also enhances dipping reflectors (Figure 5.3(a)).

In order to optimally enhance discontinuous features, it is important to orient the filter along local slopes. I compute the structural dip in the inline (Figure 5.2(a)) and crossline (Figure 5.2(b)) directions using accelerated plane-wave destruction (Chen et al., 2013a). Using the local slopes, I apply structure-oriented smoothing to enhance seismic structures and attenuate noise without blurring geologic edges (Liu et al., 2010). I subsequently apply the proposed plane-wave Sobel filter and compute the magnitude of the inline and crossline plane-wave Sobel images. Discontinuous geologic features, most prominently faults and channels, are enhanced, revealing subtle details which would be difficult to interpret from the original seismic image (Figure 3b).

I compute a more segmented image by cascading another iteration of filtering to the Sobel image, this time orienting the filter along both the dip of seismic reflections and the azimuth of the faults and channels. The plane-wave Sobel filter is applied to the Sobel filter image using structural information derived from the original seismic image. I compute linear combinations of these inline and crossline images weighted by the cosine and sine of the azimuth. The local azimuth of the faults and channels corresponds to the orientation which creates the optimal image at each point (Figure 5.2(c)). Faults and channels are further segmented in the cascaded image by automatically orienting the Sobel filter along geologic structures (Figure 5.3(c)).

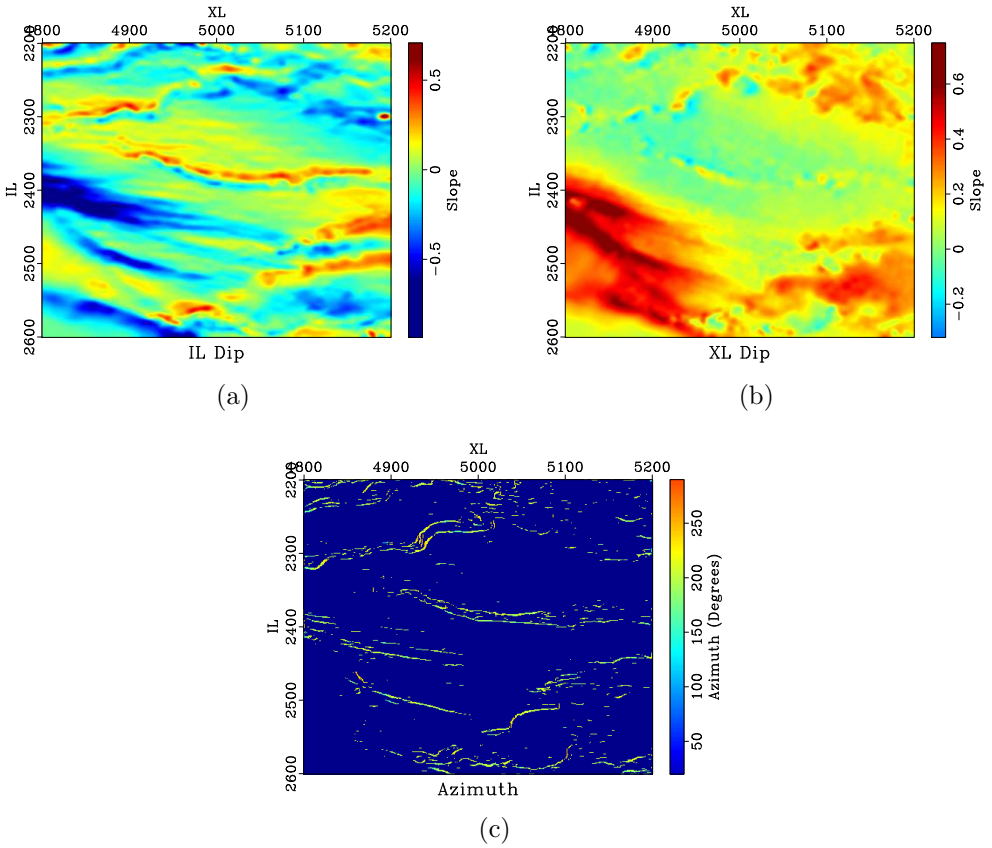

(a) (b) (c)

Figure 5.2: (a) Inline and (b) crossline reflection slopes computed using accelerated plane-wave destruction and (c) azimuth of faults and channels estimated using azimuthal plane-wave destruction. ch05-sobel/pari idip,xdip,az

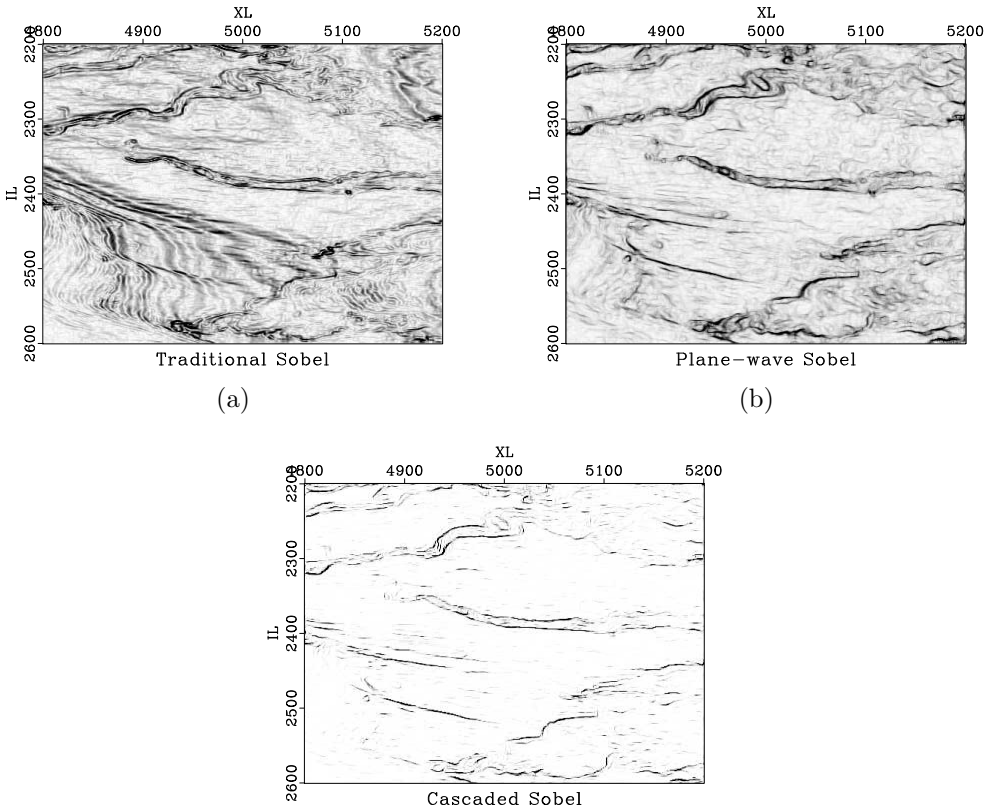

Figure 5.3: (a) The traditional Sobel filter, (b) proposed plane-wave Sobel filter, and (c) cascaded plane-wave Sobel filter applied to the Parihaka seismic data. ch05-sobel/pari flat,sobel,slice

EXAMPLE II

The next example is a subset of the Penobscot data used previously by Kington (2015) (Figure 5.4). This small marine 3D seismic volume was acquired offshore Nova Scotia, Canada and is available in the SEG open data repository (`http://wiki.seg.org/wiki/Penobscot_3D`).

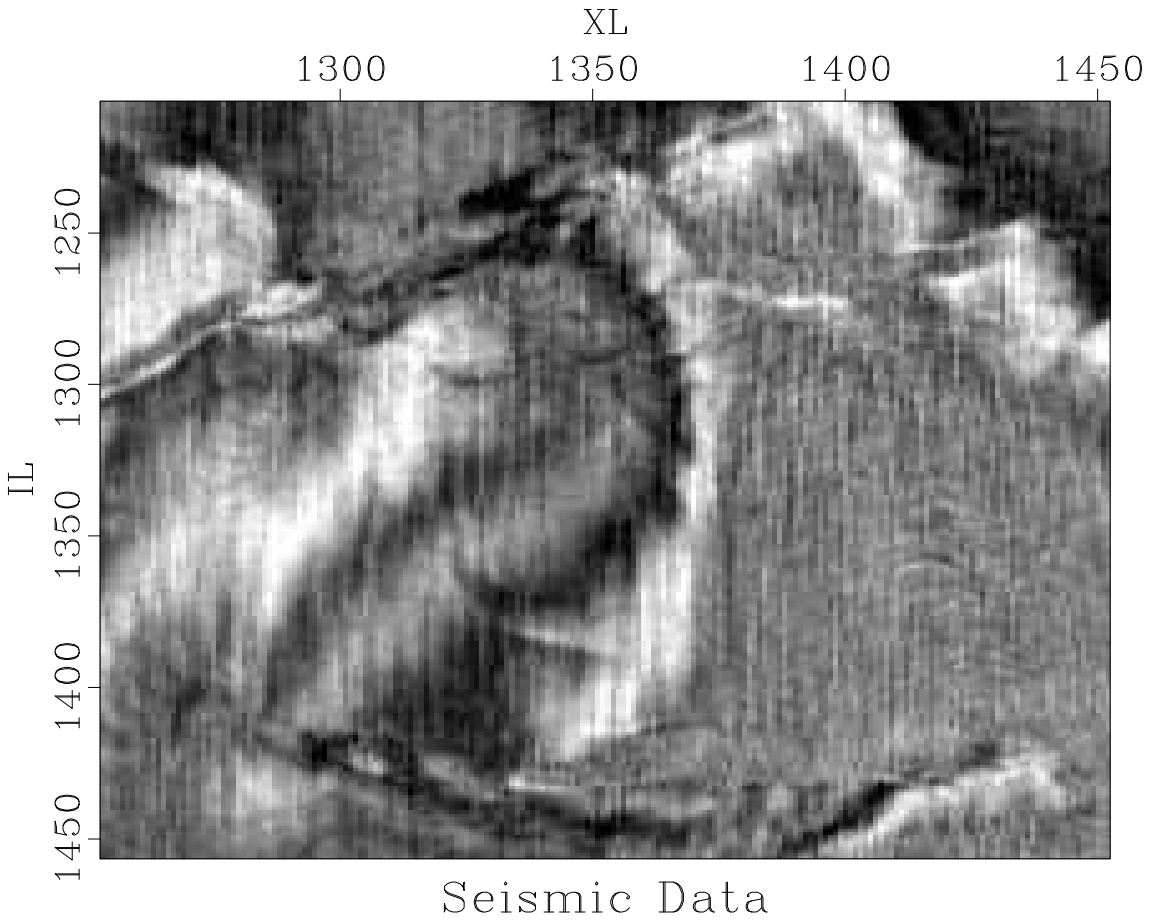

Figure 5.4: Penobscot 3D seismic data ch05-sobel/pen pen

I apply cross-correlation coherence, semblance, eigenstructure coherence, gradient-structure-tensor (GST) coherence, and predictive coherence attributes to the data and compare the results to the proposed plane-wave Sobel attribute. Correlation-based

coherence attributes (Bahorich and Farmer, 1995) produce an image of normalized local cross-correlation between adjacent seismic traces and combines them to estimate coherence. This attribute is more efficient than most of the alternative coherence attributes, but lacks robustness and has poor vertical resolution (Figure 5.5(a)). Semblance (Marfurt et al., 1998) provides better vertical resolution by incorporating a local window of traces (Figure 5.5(b)). Eigendecomposition of the local covariance matrix (Gersztenkorn and Marfurt, 1999) or gradient-structure-tensor (Randen et al., 2000) allows information about local structures to be incorporated into the coherence calculation. These attributes provide significantly better vertical and lateral resolution (Figures 5.5(c) and 5.5(d)) compared to correlation-based coherence; however, calculation and decomposition of the local covariance matrix or gradient-structure-tensor introduces significant computational cost. Furthermore, all of these attributes contain some noise contamination in coherent sections of the image. Predictive coherence (Karimi et al., 2015) uses plane-wave destruction to compute residuals between adjacent traces predicted by painting along local slopes. Discontinuities are enhanced in this image with minimal noise contamination compared to the previous attributes (Figure 5.5(e)).

I compare these results to the proposed plane-wave Sobel attributes. As expected, the filter enhances the faults and channels in the seismic image without significant noise contamination or highlighting continuous dipping reflectors (Figure 5f).

CONCLUSIONS

I have modified the Sobel filter by orienting it along the dip of seismic reflections and the azimuth of discontinuous features. I find that the proposed plane-wave Sobel filter is a straightforward and inexpensive means for enhancing discontinuous

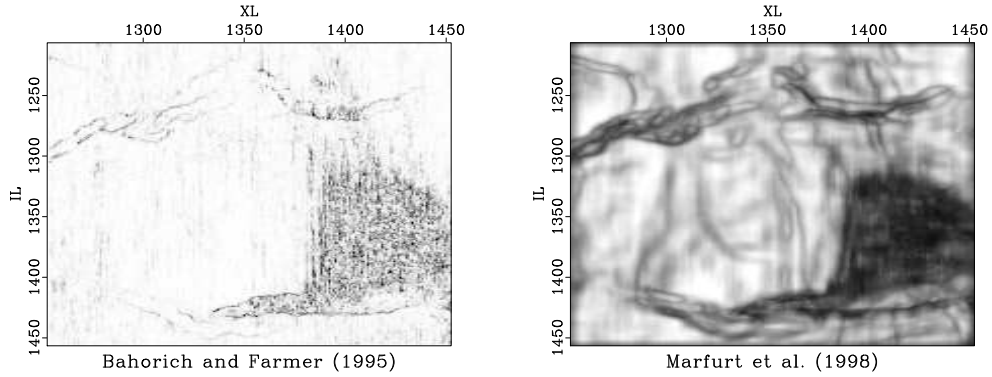

(a) (b)

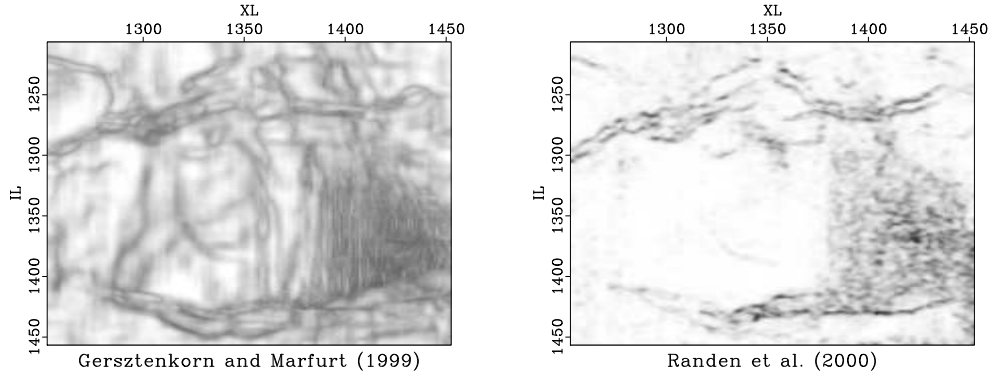

(c) (d)

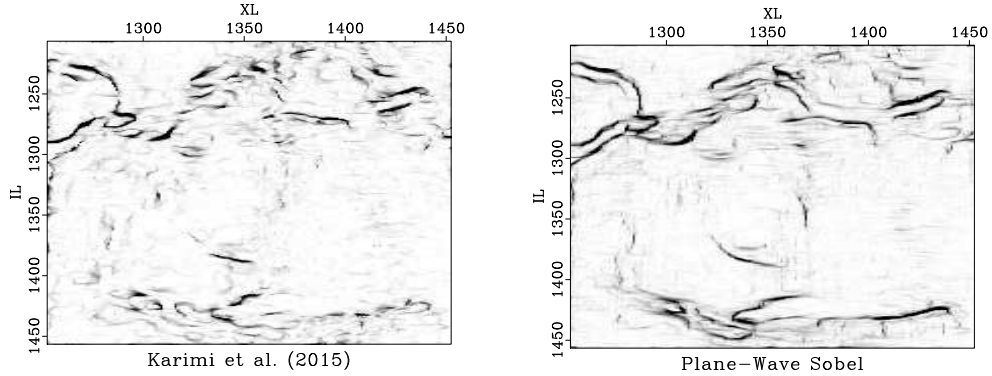

(e) (f)

Figure 5.5: Comparison of discontinuity enhancement attributes: (a) cross-correlation, (b) semblance, (c) eigenstructure, (d) gradient-structure-tensor, and (e) predictive coherence, and the (f) plane-wave Sobel filter. ch05-sobel/pen coh0,coh1,coh2,coh,pcoh,sobel

features in 3D seismic images. Many popular coherence attributes come with considerable computational cost because they require calculation and eigendecomposition of the local covariance matrix or structure tensor at each point in the 3D image. The significant cost of eigendecomposition can be partially alleviated in practice by parallelization. One of the key benefits of this method is its superior efficiency in comparison with other similar attributes. The main costs of this attribute are the estimation of local slopes and azimuth scanning. Local slopes can be estimated using accelerated plane-wave destruction. The additional azimuth scanning and picking is easy to parallelize. As demonstrated in this paper, the proposed plane-wave Sobel attribute can help geological interpretations of subsurface faults and channels. It can also be used to enhance other discontinuous or chaotic features commonly interpreted in seismic images, such as unconformities, salt boundaries, and mass transport complexes.

Chapter 6

Conclusions

In this thesis, I proposed two modifications of plane-wave destruction filters: amplitude-adjusted plane-wave destruction filters and plane-wave Sobel filters.

The proposed amplitude-adjusted plane-wave destruction algorithm utilizes a modification of plane-wave destruction filters to acquire a regularized estimate of high-resolution shifting and scaling functions between seismic traces. Plane-wave destruction is particularly effective for measuring small shifts. When shifts are small, amplitude-adjusted plane-wave destruction can be used as a standalone algorithm to efficiently measure shifting and scaling functions between seismic images. When shifts are large, the proposed algorithm can be used to refine shift predictions from other registration algorithms. Separating scaling and shifting allows local shifts to be measured more precisely. The proposed algorithm has immediate applications to time-lapse image registration, multicomponent image registration, automatic gather flattening, automatic seismic-well ties, and image merging.

As briefly discussed in chapter 3, the current implementation of amplitude-adjusted plane-wave destruction filters assumes only vertical timeshifts. Hale et al. (2008), Hale (2009a), and Cox and Hatchell (2008) show that lateral timeshifts are observed between time-lapse seismic images. For future research, I suggest implementing amplitude-adjusted omnidirectional plane-wave destruction (Chen et al., 2013b) for estimation of multidimensional time-lapse timeshifts. Furthermore, MacBeth et al.

(2016) evaluates the problem of spurious timeshifts estimates apparent in time-lapse seismic images associated with tuning effects. Phillips and Fomel (2017a) partially alleviates this problem by decomposing time-lapse seismic images into discrete frequency components using the local time-frequency transform (Liu and Fomel, 2013). For future research, I suggest to use the local time-frequency transform to perform non-stationary deconvolution (Zhang and Fomel, 2016). This may further alleviate the problem of spurious timeshifts between time-lapse seismic images.

I have also modified the Sobel filter by orienting it along the dip of seismic reflections and the azimuth of discontinuous features. I find that the proposed plane-wave Sobel filter is a straightforward and inexpensive means for enhancing discontinuous features in 3D seismic images. Many popular coherence attributes come with significant computational cost because they require calculation and eigendecomposition of the local covariance matrix or structure tensor at each point in the 3D image. One of the key benefits of the plane-wave Sobel filter is its superior efficiency in comparison with other similar attributes. The main costs of this attribute are the estimation of local slopes and azimuth scanning. Local slopes can be estimated efficiently using accelerated plane-wave destruction and azimuth scanning is easy to parallelize. As demonstrated in this thesis, the proposed plane-wave Sobel attribute can help expedite and improve geological interpretations of subsurface faults and channels. This attribute can likely be used to enhance other discontinuous or chaotic features commonly interpreted in seismic images, such as unconformities, salt boundaries, and mass transport complexes.

For further research, I suggest replacing the azimuth scanning workflow with a steerable implementation of the plane-wave Sobel filter. Furthermore, structural smoothing may be improved by incorporating non-stationary smoothing where the

radius is weighted by the magnitude of the plane-wave Sobel attribute. This will effectively smooth seismic amplitudes along continuous structures while preserving discontinuous features which may be critical for interpretation.

Bibliography

Alkhalifah, T., and I. Tsvankin, 1995, Velocity analysis for transversely isotropic media: Geophysics, **60**, 1550–1566.

Aqrawi, A. A., 2014, Adaptive Sobel based edge detection for enhaced fault segmentation: IPTC 2014: International Petroleum Technology Conference, 1424–1428.

Aqrawi, A. A., and T. H. Boe, 2011, Improved fault segmentation using a dip guided and modified 3D Sobel filter: 86th Annual International Meeting, SEG Expanded Abstracts, Society of Exploration Geophysicists, 999–1003.

Aqrawi, A. A., T. H. Boe, S. Barros, et al., 2011, Detecting salt domes using a dip guided 3D Sobel seismic attribute: 80th Annual International Meeting, SEG Expanded Abstracts, Society of Exploration Geophysicists, 1014–1018.

Baek, H., H. Calandra, and L. Demanet, 2014, Velocity estimation via registration-guided least-squares inversion: Geophysics, **79**, R79–R89.

Bahorich, M. S., and S. Farmer, 1995, 3-D seismic discontinuity for faults and stratigraphic features: The coherence cube: The Leading Edge, **14**, 1053–1058.

Bakker, P., 2002, Image structure analysis for seismic interpretation: Delft University of Technology.

Bar-Shalom, Y., 1990, Multitarget-multisensor tracking: advanced applications: Norwood, MA, Artech House, 1990, 391 p.

Barnes, A. E., 2016, Handbook of poststack seismic attributes.

Berron, C., L. Michou, B. De Cacqueray, F. Duret, J. Cotton, and E. Forgues, 2015, Permanent, continuous & unmanned 4D seismic monitoring: Peace river case study: 2015 SEG Annual Meeting.

Castagna, J. P., H. W. Swan, and D. J. Foster, 1998, Framework for AVO gradient and intercept interpretation: Geophysics, **63**, 948–956.

Chen, Z., S. Fomel, and W. Lu, 2013a, Accelerated plane-wave destruction: Geophysics, **78**, V1–V9.

———, 2013b, Omnidirectional plane-wave destruction: Geophysics, **78**, V171–V179.

Chopra, S., R. Kumar, and K. J. Marfurt, 2014, Seismic discontinuity attributes and Sobel filtering: 84th Annual International Meeting, SEG Expanded Abstracts, Society of Exploration Geophysicists, 1624–1628.

Chopra, S., and K. J. Marfurt, 2007, Seismic attributes for prospect identification and reservoir characterization: Society of Exploration Geophysicists Tulsa, USA.

Claerbout, J. F., 1992, Earth soundings analysis: Processing versus inversion: Blackwell Scientific Publications Cambridge, Massachusetts, USA, **6**.

Cohen, I., N. Coult, and A. A. Vassiliou, 2006, Detection and extraction of fault surfaces in 3D seismic data: Geophysics, **71**, P21–P27.

Cox, B., and P. Hatchell, 2008, Straightening out lateral shifts in time-lapse seismic: First Break, **26**.

Fomel, S., 2002, Applications of plane-wave destruction filters: Geophysics, **67**, 1946–1960.

———, 2007a, Local seismic attributes: Geophysics, **72**, A29–A33.

———, 2007b, Shaping regularization in geophysical-estimation problems: Geophysics, **72**, R29–R36.

———, 2007c, Velocity-independent time-domain seismic imaging using local event slopes: Geophysics, **72**, S139–S147.

———, 2009, Velocity analysis using AB semblance: Geophysical Prospecting, **57**, 311–321.

———, 2010, Predictive painting of 3D seismic volumes: Geophysics, **75**, A25–A30.

Fomel, S., M. Backus, K. Fouad, B. Hardage, G. Winters, et al., 2005, A multistep approach to multicomponent seismic image registration with application to a West Texas carbonate reservoir study: 2005 SEG Annual Meeting.

Fomel, S., and L. Jin, 2009, Time-lapse image registration using the local similarity attribute: Geophysics, **74**, A7–A11.

Fomel, S., P. Sava, I. Vlad, Y. Liu, and V. Bashkardin, 2013, Madagascar: Open-source software project for multidimensional data analysis and reproducible computational experiments: Journal of Open Research Software, **1**, 1–4.

Fowler, P., and J. F. Claerbout, 1983, Tpow: An estimator of seismic amplitude decay: SEP-38: Stanford Exploration Project, 73–88.

Gersztenkorn, A., and K. J. Marfurt, 1999, Eigenstructure-based coherence computations as an aid to 3-D structural and stratigraphic mapping: Geophysics, **64**, 1468–1479.

Golub, G. H., and V. Pereyra, 1973, The differentiation of pseudo-inverses and nonlinear least squares problems whose variables separate: SIAM Journal on numerical analysis, **10**, 413–432.

Greer, S., and S. Fomel, 2017, Matching and merging high-resolution and legacy seismic images: Presented at the 87th Annual International Meeting, SEG Expanded Abstracts, Society of Exploration Geophysicists. (submitted).

Gulunay, N., M. Magesan, and H. Roende, 2008, Gather flattening based on event tracking for each time sample: Presented at the 70th EAGE Conference and Exhibition incorporating SPE EUROPEC 2008.

Hale, D., 2006, Fast local cross-correlations of images, *in* 76th Annual International

Meeting, SEG Expanded Abstracts: Society of Exploration Geophysicists, 3160–3164.

———, 2009a, A method for estimating apparent displacement vectors from time-lapse seismic images: Geophysics, **74**, V99–V107.

———, 2009b, Structure-oriented smoothing and semblance: CWP-635, 261–270.

———, 2013a, Dynamic warping of seismic images: Geophysics, **78**, S105–S115.

———, 2013b, Methods to compute fault images, extract fault surfaces, and estimate fault throws from 3D seismic images: Geophysics, **78**, 33–43.

Hale, D., B. Cox, and P. Hatchell, 2008, Apparent horizontal displacements in time-lapse seismic images, *in* 78th Annual International Meeting, SEG Expanded Abstracts: Society of Exploration Geophysicists, 3169–3173.

Hardage, B. A., M. V. DeAngelo, P. E. Murray, and D. Sava, 2011, Multicomponent seismic technology.

Hatchell, P., and S. Bourne, 2005, Rocks under strain: Strain-induced time-lapse time shifts are observed for depleting reservoirs: The Leading Edge, **24**, 1222–1225.

Herrera, R. H., S. Fomel, and M. van der Baan, 2014, Automatic approaches for seismic to well tying: Interpretation, **2**, SD9–SD17.

Herrera, R. H., and M. van der Baan, 2012, Guided seismic-to-well tying based on dynamic time warping: 2012 SEG Annual Meeting, 1–5.

Hinkley, D., G. W. Bear, and C. Dawson, 2004, Prestack gather flattening for AVO: 74th Ann. Internat. Mtg.: Soc. of Expl. Geophys, **2329**, 2329.

Hoeber, H., S. Campbell, M. Dyce, and D. Whitecombe, 2008, Using complex trace analysis for 4D matching and 4D noise reduction: First Break, **26**.

Horn, B. K. P., and B. G. Schunck, 1981, Determining optical flow: Artificial intelligence, **17**, 185–203.

Kanu, C., A. Toomey, L. Hodgson, M. Gherasim, E. L'Heureux, B. Du, and Q. Zhang, 2016, Evaluation of time-shift extraction methods on a synthetic model with 4d geomechanical changes: The Leading Edge, **35**, 888–893.

Karimi, P., and S. Fomel, 2015, Stratigraphic coordinates: A coordinate system tailored to seismic interpretation: Geophysical Prospecting, **63**, 1246–1255.

Karimi, P., S. Fomel, L. Wood, and D. Dunlap, 2015, Predictive coherence: Interpretation, **3**, SAE1–SAE7.

Karimi, P., S. Fomel, and R. Zhang, 2016, Time-lapse image registration using the stratigraphic-coordinate system, *in* 86th Annual International Meeting, SEG Expanded Abstracts: Society of Exploration Geophysicists, 5500–5505.

Kaufman, L., 1975, A variable projection method for solving separable nonlinear least squares problems: BIT Numerical Mathematics, **15**, 49–57.

Keys, R. G., and D. J. Foster, 1998, A data set for evaluating and comparing seismic inversion methods: Comparison of seismic inversion methods on a single real data set, 1–12.

Kim, T., and Y. Im, 2003, Automatic satellite image registration by combination of matching and random sample consensus: IEEE transactions on geoscience and remote sensing, **41**, 1111–1117.

Kington, J., 2015, Semblance, coherence, and other discontinuity attributes: The Leading Edge, **34**, 1510–1512.

Lie, E., 2011, Constrained timeshift estimation: Presented at the 73rd EAGE Conference and Exhibition incorporating SPE EUROPEC 2011.

Liu, Y., and S. Fomel, 2013, Seismic data analysis using local time-frequency decomposition: Geophysical Prospecting, **61**, 516–525.

Liu, Y., S. Fomel, and G. Liu, 2010, Nonlinear structure-enhancing filtering using plane-wave prediction: Geophysical Prospecting, **58**, 415–427.

Lumley, D. E., 2001, Time-lapse seismic reservoir monitoring: Geophysics, **66**, 50–53.

Luo, Y., W. G. Higgs, and W. S. Kowalik, 1996, Edge detection and stratigraphic analysis using 3D seismic data: 66th Annual International Meeting, SEG Expanded Abstracts, Society of Exploration Geophysicists, 324–327.

MacBeth, C., M.-D. Mangriotis, and P. Hatchell, 2016, Evaluation of the spurious time-shift problem, *in* 86th Annual International Meeting, SEG Expanded Abstracts: Society of Exploration Geophysicists, 5457–5462.

Maintz, J. A., and M. A. Viergever, 1998, A survey of medical image registration: Medical image analysis, **2**, 1–36.

Marfurt, K. J., R. L. Kirlin, S. L. Farmer, and M. S. Bahorich, 1998, 3-D seismic attributes using a semblance-based coherency algorithm: Geophysics, **63**, 1150–1165.

Merzlikin, D., S. Fomel, and A. Bona, 2016, Diffraction imaging using azimuthal plane-wave destruction: 86th Annual International Meeting, SEG Expanded Abstracts, Society of Exploration Geophysicists, 4288–4293.

Merzlikin, D., F. S, X. Wu, and M. Phillips, 2017, Unconventional reservoir characterization using azimuthal plane-wave destruction seismic diffraction imaging workflow: Presented at the Unconventional Resources Technology Conference, Austin, TX, 24-26 July 2017, Society of Exploration Geophysicists, American Association of Petroleum Geologists, Society of Petroleum Engineers. (submitted).

Munoz, A., and D. Hale, 2012, Automatically tying well logs to seismic data: Center for Wave Phenomena, Colorado School of Mines, Golden, CO80401, USA, 253–260.

Nuth, C., and A. Kääb, 2011, Co-registration and bias corrections of satellite elevation data sets for quantifying glacier thickness change: The Cryosphere, **5**, 271.

O'Gorman, L., M. J. Sammon, and M. Seul, 2008, Practical algorithms for image analysis: Cambridge University Press.

Phillips, M., 2017, Automatic gather flattening using amplitude-adjusted plane-wave destruction filters, *in* 87th Annual International Meeting, SEG Expanded Abstracts: Society of Exploration Geophysicists. (submitted).

Phillips, M., and S. Fomel, 2016, Seismic time-lapse image registration using amplitude-adjusted plane-wave destruction, *in* 86th Annual International Meeting, SEG Expanded Abstracts: Society of Exploration Geophysicists, 5473–5478.

———, 2017a, Estimation of timeshifts in time-lapse seismic images using spectral decomposition, *in* 87th Annual International Meeting, SEG Expanded Abstracts: Society of Exploration Geophysicists. (submitted).

———, 2017b, Plane-wave sobel attribute for discontinuity enhancement in seismic images: Geophysics. (in review).

Phillips, M., S. Fomel, and R. Swindeman, 2016, Structure-oriented plane-wave Sobel filter for edge detection in seismic images: 86th Annual International Meeting, SEG Expanded Abstracts, Society of Exploration Geophysicists, 1954–1959.

Qian, F., L. Chen, F. Zhang, and G. Hu, 2016, Prestack gather flattening using segmental dynamic time warp, *in* 86th Annual International Meeting, SEG Expanded Abstracts: Society of Exploration Geophysicists, 592–596.

Randen, T., E. Monsen, C. Signer, A. Abrahamsen, J. O. Hansen, T. Sæter, J. Schlaf, and L. Sønneland, 2000, Three-dimensional texture attributes for seismic data analysis: 70th Annual International Meeting, SEG Expanded Abstracts, 668–671.

Randen, T., S. I. Pedersen, and L. Sonneland, 2001, Automatic extraction of fault surfaces from three-dimensional seismic data: 71st Annual International Meeting, SEG Expanded Abstract, 551–554.

Rickett, J. E., and D. E. Lumley, 2001, Cross-equalization data processing for time-lapse seismic reservoir monitoring: A case study from the gulf of mexico: Geophysics, **66**, 1015–1025.

Sakoe, H., and S. Chiba, 1978, Dynamic programming algorithm optimization for spoken word recognition: Acoustics, Speech and Signal Processing, IEEE Transactions on, **26**, 43–49.

Shuey, R., 1985, A simplification of the Zoeppritz equations: Geophysics, **50**, 609–614.

Sobel, I., and G. Feldman, 1968, A 3x3 isotropic gradient operator for image processing: Stanford Artificial Project, 271–272.

Swindeman, R., and S. Fomel, 2015, Seismic data interpolation using plane-wave shaping regularization: 85th Annual International Meeting, SEG Expanded Abstract, Society of Exploration Geophysicists, 3853–3858.

Taner, M. T., and F. Koehler, 1981, Surface consistent corrections: Geophysics, **46**, 17–22.

Taner, M. T., F. Koehler, and R. Sheriff, 1979, Complex seismic trace analysis: Geophysics, **44**, 1041–1063.

Thiran, J.-P., 1971, Recursive digital filters with maximally flat group delay: IEEE Transactions on Circuit Theory, **18**, 659–664.

Tsvankin, I., 1997, Reflection moveout and parameter estimation for horizontal transverse isotropy: Geophysics, **62**, 614–629.

Verschuur, D. J., A. Berkhout, and C. Wapenaar, 1992, Adaptive surface-related multiple elimination: Geophysics, **57**, 1166–1177.

Williamson, P. R., A. J. Cherrett, and P. A. Sexton, 2007, A new approach to warping for quantitative time–lapse characterisation: 69th EAGE Conference and Exhibition incorporating SPE EUROPEC 2007.

Wu, X., 2017, Directional structure-tensor-based coherence to detect seismic faults and channels: Geophysics, **82**, A13–A17.

Wu, X., and G. Caumon, 2016, Simultaneous multiple well-seismic ties using flattened synthetic and real seismograms: Geophysics, **82**, IM13–IM20.

Wu, X., and D. Hale, 2016, 3D seismic image processing for faults: Geophysics, **81**, IM1–IM11.

Wu, X., S. Luo, and D. Hale, 2016, Moving faults while unfaulting 3D seismic images: Geophysics, **81**, IM25–IM33.

Zhang, Q., and B. Du, 2016, Multiscale and iterative refinement optical flow (MSIROF) for seismic image registration and gather flattening using multidimensional shifts, *in* 86th Annual International Meeting, SEG Expanded Abstracts: Society of Exploration Geophysicists, 5468–5472.

Zhang, R., and S. Fomel, 2016, Time-variant wavelet extraction with a local-attribute-based time-frequency decomposition for seismic inversion: Interpretation, **5**, SC9–SC16.

Zhang, R., X. Song, S. Fomel, M. K. Sen, and S. Srinivasan, 2013, Time-lapse seismic data registration and inversion for CO_2 sequestration study at Cranfield: Geophysics, **78**, B329–B338.

———, 2014, Time-lapse pre-stack seismic data registration and inversion for CO_2 sequestration study at Cranfield: Geophysical Prospecting, **62**, 1028–1039.

Vita

Mason Phillips grew up in Spring, Texas and graduated from The Woodlands College Park High School in 2012. He subsequently moved to Austin to attend the University of Texas. In 2014, he began working with the Texas Consortium for Computational Seismology (TCCS), an initiative of the Bureau of Economic Geology (BEG) and the Institute of Computational Engineering and Sciences (ICES). Upon earning a B.S. in geophysics in 2015, he chose to remain at the University of Texas at Austin to pursue his graduate degree. Later this year, he will join the Areal Monitoring Team at Shell Projects & Technology in Houston, TX.

Permanent address: 27316 S Lazy Meadow Way. Spring, TX, 77386

This thesis was typeset with LaTeX[†] by the author.

[†]LaTeX is a document preparation system developed by Leslie Lamport as a special version of Donald Knuth's TeX Program.